

1 Mapping 24 woody plant species phenology and ground forests 2 phenology over China from 1951-2020

3 Mengyao Zhu¹, Junhu Dai^{1,2,3}, Huanjiong Wang¹, Juha M. Alatalo⁴, Wei Liu^{1,2}, Yulong Hao^{1,2},
4 Quansheng Ge^{1,2}

5 ¹Key Laboratory of Land Surface Pattern and Simulation, Institute of Geographic Sciences and Natural Resources Research,
6 Chinese Academy of Sciences, Beijing, 100101, China

7 ²College of Resources and Environment, University of Chinese Academy of Sciences, Beijing, 101408, China

8 ³China-Pakistan Joint Research Center on Earth Sciences, CAS-HEC, Islamabad, 45320, Pakistan

9 ⁴Environmental Science Centre, Qatar University, Doha, 2713, Qatar

10 *Correspondence to:* Junhu Dai (daijh@igsnrr.ac.cn); Quansheng Ge (geqs@igsnrr.ac.cn)

11 **Abstract.** Plant phenology refers to the cyclic plant growth events, and is one of the most important indicators of climate
12 change. Integration of plant phenology information is of great significance for understanding the response of ecosystems to
13 global change and simulating the material and energy balance of terrestrial ecosystems. Based on 24552 in-situ phenology
14 observation records of 24 typical woody plants from the Chinese Phenology Observation Network (CPON), we map the
15 species phenology (SP) and ground phenology (GP) of forests over China from 1951-2020, with a spatial resolution of 0.1°
16 and a temporal resolution of 1 day. A model-based upscaling method was used to generate SP maps from in-situ
17 **SPphenology** observations, and then weighted average and quantile methods were used to generate GP maps from SP maps.
18 The validation shows that the SP maps of 24 woody plants are largely consistent with the in-situ observations, with an
19 average error of 6.9 days in spring and 10.8 days in autumn. The GP maps of forests have good agreement with the existing
20 Land Surface Phenology (LSP) products derived by remote sensing data, particularly in deciduous forests, with an average
21 difference of 8.8 days in spring and 15.1 days in autumn. The dataset provides an independent and reliable phenology data
22 source on a long-time scale of 70 years in China, and contributes to more comprehensive research on plant phenology and
23 climate change at regional and national scales. The dataset can be accessed at <https://doi.org/10.57760/sciencedb.07995> (Zhu
24 et al., 2023).

25 1 Introduction

26 Plant phenology refers to plant cyclic growth and development events, which are formed by adaptation to seasonal
27 changes in climate and environmental conditions (Lieth, 1974; Schwartz, 2003). These phenological events include critical
28 stages such as budburst, leaf unfolding, flowering, leaf coloring, and defoliation. As a highly sensitive biological indicator of
29 climate change (Fu et al., 2015; Richardson et al., 2013), plant phenology is not only important for comprehending
30 ecosystem responses to global change (Inouye, 2022; Menzel et al., 2020), but also a significant factor in simulating material
31 and energy balance of terrestrial ecosystems (Keenan et al., 2014; Wang et al., 2020b). To be helpful for biological

32 monitoring and predictions, long-term, dependable plant phenology data on a global scale are greatly desired by related
33 scientific research personnel. Presently, such data can be procured from diverse sources (Piao et al., 2019; Tang et al., 2016),
34 including manual in-situ observations ([Schwartz et al., 2012](#); [Templ et al., 2018](#)), satellite remote sensing (Bolton et al.,
35 2020; Dixon et al., 2021), and tower-based digital cameras ([Nasahara and Nagai, 2015](#); [Richardson et al., 2018](#)), etc.
36 Nevertheless, integrating large-scale and long-term plant phenology information continues to pose a formidable challenge,
37 owing to the substantial gaps in spatial and temporal scales between different data sources (Fisher et al., 2006; Park et al.,
38 2021).

39 The practice of conducting manual, in-situ observations for species phenology (SP) boasts a rich history spanning
40 several centuries (Aono and Kazui, 2008), yielding precise phenological information for the individual plant species (Polgar
41 and Primack, 2011). In 1963, the Chinese Academy of Sciences inaugurated the Chinese Phenology Observation Network
42 (CPON), a standardized, nationwide network employing a multitude of professional observers and incorporating extensive
43 ground-based observations. To date, CPON has amassed over 1.2 million [SPphenology](#) records pertaining to more than 900
44 plant species across over 150 sites throughout China (Fig. 1), cementing its dominant status as a data center for phenological
45 research in China. These [phenologySP](#) records have been contributed to examining the spatiotemporal patterns of plant
46 phenological shifts (Dai et al., 2014; Ge et al., 2015), the environmental determinants influencing plant phenology (Dai et
47 al., 2013; Wang et al., 2020a), as well as the development of phenology models in China (Tao et al., 2018; [Wang et al., 2015](#)).
48 Nonetheless, the spatial coverage of in-situ [phenologySP](#) data remains sporadic and restricted on regional and global
49 scales (Donnelly et al., 2022), with noticeable gaps appearing in longer time scales. The progression of species-level
50 phenology modeling presents an opportunity to address these limitations (Fu et al., 2020; Hufkens et al., 2018). In the
51 absence of actual observed [phenologySP](#) data, phenology models can be employed to generate large-scale predictions,
52 thereby interpolating the missing [SP](#)-data in both space and time (Cleland et al., 2007; [Schwartz et al., 2013](#); Wang et al.,
53 2012). For instance, the Extended Spring Indices (SI-x) model has been successfully applied to create gridded maps
54 illustrating the first leaf and first bloom events for three woody plants at a resolution ranging from 1° to 1 km across the
55 contiguous United States (Ault et al., 2015; Izquierdo-Verdiguier et al., 2018). Similarly, this model-based approach can be
56 adapted to model and map the SP data throughout China. This would enable the integration and synthesis of CPON's long-
57 term phenology observations at regional and national scales within the country.

58 In contrast to manual in-situ observations, satellite remote sensing facilitates the monitoring and mapping of land
59 surface phenology (LSP) on a more expansive scale. It provides more comprehensive LSP information at the landscape level
60 (Studer et al., 2007). Over the past four decades, remote sensing technology has witnessed considerable advancements,
61 significantly improving the spatial and temporal resolution (Misra et al., 2020; Dronova and Taddeo, 2022). At present, a
62 multitude of LSP products derived from vegetation indices (e.g., NDVI and EVI) procured from multi-source remote sensing
63 data are accessible, offering regional and global LSP data with varying spatial resolutions ranging from 10 km to 30 m (e.g.,
64 [Ganguly et al., 2010](#); Li et al., 2019; Wu et al., 2021; [Zhang et al., 2020](#)). The credibility of these LSP data remains largely
65 contingent upon ground phenology (GP) validation based on in-situ observed SP data (Tian et al., 2021; Zhang et al., 2017),

66 particularly the coordination and aggregation from individual-level phenology (i.e., SP) to landscape-level phenology (i.e.,
67 GP). Weighted average and quantile methods have been proven effective for aggregating phenology from individual to
68 community or landscape levels (Donnelly et al., 2022; Fitchett et al., 2015). Prior research has validated weighted average
69 method on a site scale through field investigations and remote sensing monitoring, to aggregate GP at the community or
70 landscape levels from in-situ SP data weighted by species abundance (Liang et al., 2011). Some recent studies have
71 suggested that the quantile method (e.g., 30th percentile) holds greater promise than the commonly used average method on
72 a larger scale, as evidenced in Europe and the USA (Ye et al., 2022). However, there is no previous study endeavored to
73 employ these methods for aggregating large-scale GP from SP data in China, which may constrain the availability of ground
74 validation evidence for LSP products and hinder comprehensive understanding of the spatio-temporal characteristics of
75 phenological changes over the country.

76 In this study, we aimed to develop long-term SP and GP maps of China with a 0.1° resolution spanning 1951-2020,
77 supplying spatially continuous grided phenology products currently absent in the country and crucial for a wider array of
78 applications. We utilized 24,552 in-situ phenology observations of 24 representative woody plants from 122 sites over the
79 past six decades from CPON. Three phenophases, namely the first leaf date (FLD), first flower date (FFD), and 100% leaf
80 coloring date (LCD), were included for each species. We employed five species-level phenology models and grided
81 meteorological data to simulate and produce SP maps, and utilized species distribution maps as masks of SP maps for each
82 corresponding plant species. We applied weighted average and quantile methods on SP maps to aggregate and produce GP
83 maps, which used the distribution probabilities of each species as weights. The accuracy of SP maps was assessed through
84 cross-validation, while the reliability of GP maps was evaluated by comparing them with existing LSP products. This study
85 introduces a novel grid phenology dataset for China, which supplements China's existing phenology data sources and
86 provides an independent phenology data source for LSP product verification. The dataset will facilitate more comprehensive
87 research on plant phenology and global change by better characterizing the spatiotemporal patterns of plant phenology.

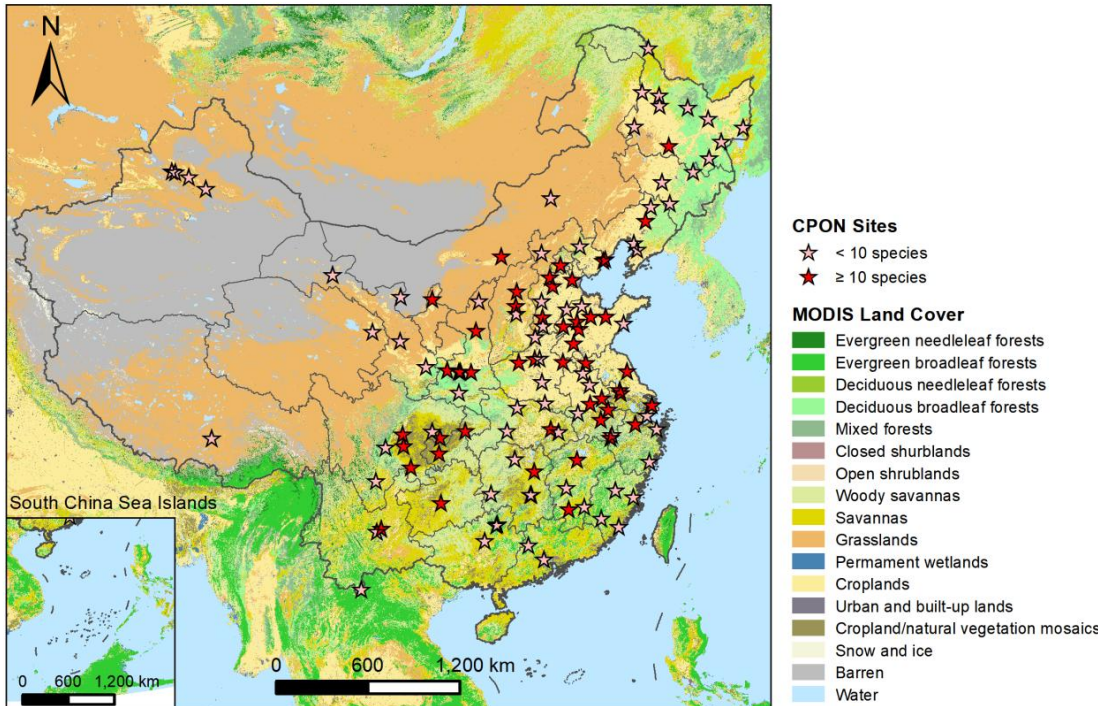
88 **2 Methods**

89 **2.1 Data acquisition and processing**

90 **2.1.1 Phenology observations**

91 The in-situ phenology observations from 1963 to 2018 were obtained from the CPON. We selected 24 species of woody
92 plants from 17 families in China (Table 1) that are common and widespread in forest ecosystems in China (Fang et al., 2011)
93 and well-documented in CPON. These species have been observed over 55 years in 122 sites, with a total of 24,552 records,
94 covering a range of land cover, ecological, and climatic conditions across China (Fig. 1). Each species had at least 40 years
95 and 13 sites of phenology data. We extractedstudied three phenophases for each species: spring FLD, spring FFD, and
96 autumn LCD. Three-sigma limits, which refers to data within three standard deviations from a mean, was used to set the

97 upper and lower limits of phenology data for each species (Pukelsheim, 1994). We identified and removed outliers beyond
 98 the three-sigma lines, because they represented less than 1% of all data points on a standard normal distribution
 99 curve. Outliers were eliminated for each species based on the principle of three sigma limits.



100
 101 **Figure 1:** Geographic distribution of CPON sites (n = 122) included in the phenology dataset across China. Sites with less
 102 than 10 recorded species are marked with pink asterisks, while sites with more than 10 recorded species are marked with red
 103 asterisks. Note that the markings on the map of several adjacent sites may overlap each other. The background map shows
 104 the IGBP land cover type from the MODIS Land Cover product (Friedl and Sulla-Menashe, 2022).

105
 106 **Table 1:** List of 24 species of woody plants from 17 families in China. Number of records represents the total number of
 107 three phenophases (FLD, FFD and LCD) of all sites and all years for each species.

No.	Species	Family	Life form	Number of sites	Number of years	Number of records
1	<i>Ginkgo biloba</i>	Ginkgoaceae	Tree	45	49	1110
2	<i>Metasequoia glyptostroboides</i>	Cupressaceae	Tree	37	47	860
3	<i>Magnolia denudata</i>	Magnoliaceae	Tree	42	47	980

4	<i>Salix babylonica</i>	Salicaceae	Tree	65	42	1526
5	<i>Populus × canadensis</i>	Salicaceae	Tree	43	51	954
6	<i>Robinia pseudoacacia</i>	Fabaceae	Tree	54	45	1757
7	<i>Albizia julibrissin</i>	Fabaceae	Tree	36	47	984
8	<i>Cercis chinensis</i>	Fabaceae	Shrub	52	49	1207
9	<i>Prunus armeniaca</i>	Rosaceae	Tree	46	45	950
10	<i>Ulmus pumila</i>	Ulmaceae	Tree	60	44	1428
11	<i>Morus alba</i>	Moraceae	Tree	50	50	1071
12	<i>Broussonetia papyrifera</i>	Moraceae	Tree	41	43	1103
13	<i>Quercus acutissima</i>	Fagaceae	Tree	17	40	292
14	<i>Pterocarya stenoptera</i>	Juglandaceae	Tree	29	46	936
15	<i>Juglans regia</i>	Juglandaceae	Tree	50	47	816
16	<i>Betula platyphylla</i>	Betulaceae	Tree	13	43	369
17	<i>Acer pictum</i> subsp. <i>mono</i>	Sapindaceae	Tree	18	46	492
18	<i>Ailanthus altissima</i>	Simaroubaceae	Tree	34	47	873
19	<i>Melia azedarach</i>	Meliaceae	Tree	61	46	1410
20	<i>Firmiana simplex</i>	Malvaceae	Tree	57	48	1403
21	<i>Hibiscus syriacus</i>	Malvaceae	Shrub	58	47	1096
22	<i>Fraxinus chinensis</i>	Oleaceae	Tree	23	40	505
23	<i>Syringa oblata</i>	Oleaceae	Shrub	50	51	1163
24	<i>Paulownia fortunei</i>	Paulowniaceae	Tree	49	48	1267
Total		-	-	122	55	24552

108

109 **2.1.2 Climate data**

110 The daily mean temperature (T) from 1950-2020 were obtained from two sources: (1) Site T was extracted from climate
 111 observations in the China Meteorological Data Service Center (CMDSC, <https://data.cma.cn/>) and used to parameterize the
 112 phenology models. (2) Grid T was extracted from ERA5-Land climate reanalysis data (Muñoz Sabater, 2019; Muñoz-
 113 Sabater et al., 2021) from the Copernicus Climate Change Service (C3S, <https://cds.climate.copernicus.eu/>) and used for

114 phenology simulation and upscaling at a spatial resolution of 0.1° (about 10 km). Hourly grid T was averaged across four
115 phases (4:00, 10:00, 16:00, 22:00) to derive the daily grid T.

116 The current bioclimatic (BIOCLIM+) variables were obtained from Climatologies at High Resolution for the Earth
117 Land Surface Areas (CHELSA, <https://chelsa-climate.org/>) to determine the species distribution (Brun et al., 2022a, b). The
118 BIOCLIM+ variables indicate the average ecological and climatic conditions during 1981-2010, with a high resolution of
119 0.0083° . We extracted the traditional 19 bioclimatic layers (Bio1-Bio19) and the complementary 50 bioclimatic layers in
120 China. We calculated the correlation between every two layers to reduce the impact of autocorrelation among these
121 bioclimatic layers, and then excluded the layers with a correlation coefficient greater than 0.8 with the previous layers. As a
122 result, 12 bioclimatic layers were retained as the environmental data inputs for the species distribution models (Table S1).
123 These layers were resampled to 0.1° to match the resolution of the grid T data.

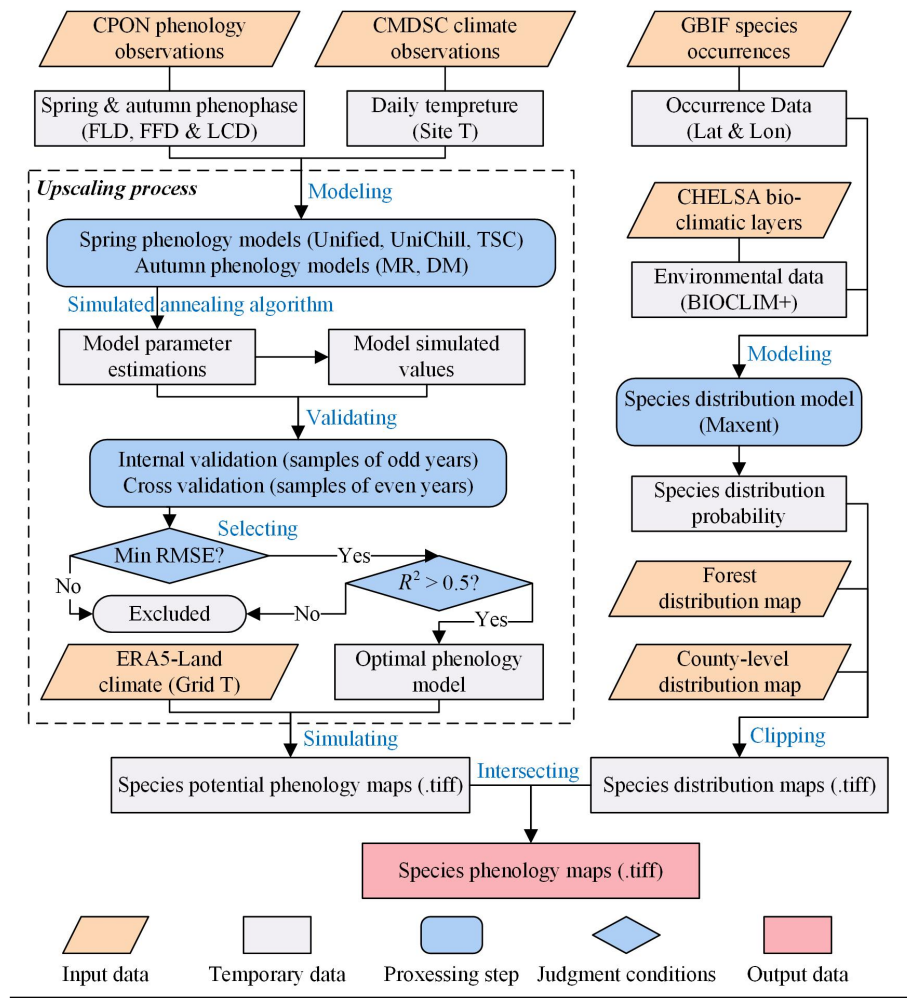
124 **2.1.3 Forest and species distribution data**

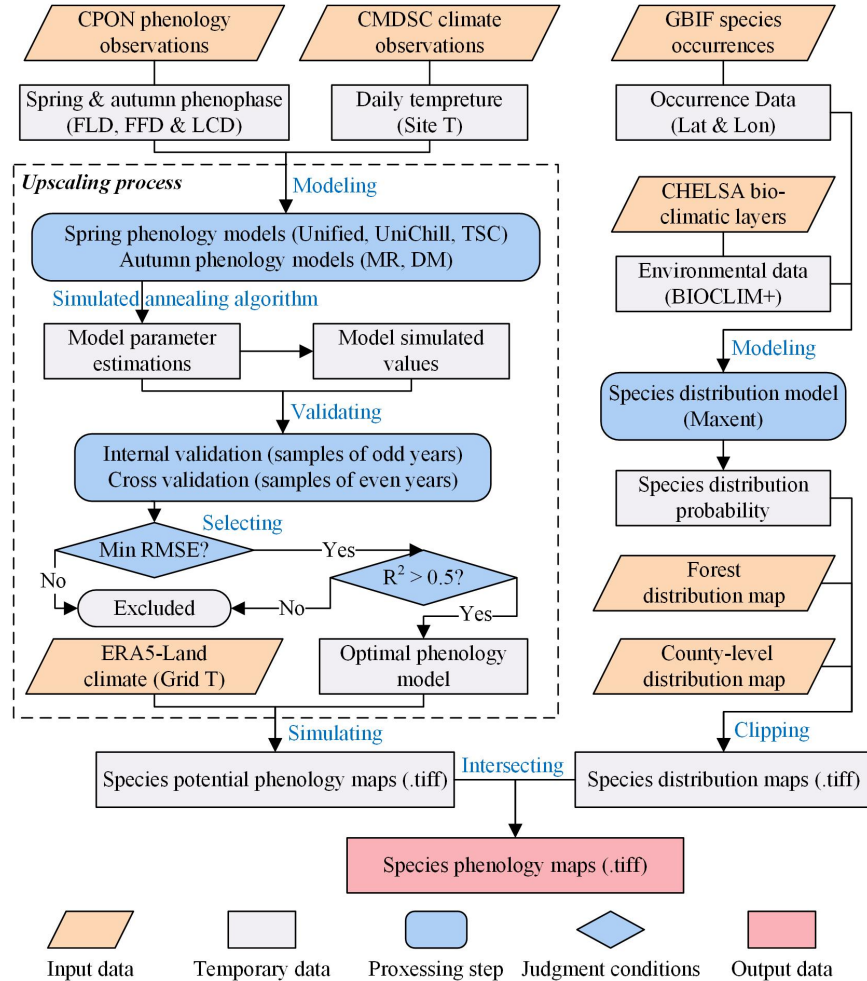
125 The forest distribution map of China was derived from the dataset of “Annual Dynamics of Global Land Cover and its
126 Long-term Changes from 1982 to 2015” (Liu et al., 2020). Each year’s land cover (LC) layers were reclassified as forest and
127 non-forest, and then the number of years of forest cover was obtained by adding all layers. Pixels with at least one year of
128 forest cover were identified as forest distribution areas. The forest types were identified from the most commonly used
129 International Geosphere-Biosphere Program (IGBP) classification from MODIS Land Cover Type (MCD12C1) Version 6.1
130 data product (Friedl and Sulla-Menashe, 2022). We merged evergreen needleleaf forest (class 1) and evergreen broadleaf
131 forest (class 2) into evergreen forest, and deciduous needleleaf forest (class 3) and deciduous broadleaf forest (class 4) into
132 deciduous forest. Mixed forest (class 5) was also included in the forest type. The forest distribution map and forest type map
133 were resampled from 0.05° to 0.1° by the majority method to match the resolution of the grid T data.

134 The county-level species distribution maps were obtained from the updated Database of China’s Woody Plants (Fang et
135 al., 2011). The distribution maps in this database were compiled from all national, provincial, and regional floras and
136 inventory reports in China published before 2009, which are considered authoritative (Cai et al., 2021). We then obtained a
137 total of 4371 occurrence records for 24 woody plant species ~~the species occurrence records~~ from the Global Biodiversity
138 Information Facility ([GBIF, 2022; https://www.gbif.org/](https://www.gbif.org/)), and used them as the occurrence
139 data inputs for the species distribution models ([GBIF, 2022](https://www.gbif.org/)). The occurrence records were filtered by including the
140 coordinate locations with uncertainty less than 2000 meters, and cleaned by removing duplicate records ([Table S2](#)).

141 **2.2 Generating species phenology maps using a model-based upscaling method**

142 The generation of species phenology maps involves two major processes: (1) Generating species potential phenology
143 maps, and (2) Generating species distribution maps. The final SP maps were obtained by spatially intersecting these two
144 maps. The workflow for the processes is shown in Fig. 2.





146

147 **Figure 2:** The workflow of generating SP maps using a model-based upscaling method, which involves two major
148 processes: (1) Generating species potential phenology maps, and (2) Generating species distribution maps. The words in blue
149 color represent the key processes of data generation. “.tiff” indicates the GeoTIFF format of the grid phenology or
150 distribution maps.

151 **2.2.1 Species potential phenology maps**

152 In the first process, we used a model-based upscaling method to convert in-situ phenology observations into grid
153 phenology maps. Phenology models were built using the phenophases (i.e., FLD, FFD, LCD) from CPON phenology
154 observations and the corresponding site T from CMDSC climate observations. For each species, we built three spring
155 phenology models: the Unichill, Unified (Chuine, 2000) and temporal-spatial coupling (TSC) models (Ge et al., 2014), and
156 two autumn phenology models: the multiple regression (MR) (Estrella and Menzel, 2006) and temperature-photoperiod (TP)

157 models (Delpierre et al., 2009). The details of the model formulae are described in Appendix S1. For each model, samples
158 from odd years were used for phenology modeling, and samples from even years were reserved for cross validation on the
159 model. All model parameters were estimated using the simulated annealing algorithm (Chuine et al., 1998).

160 For model validation, the models' root mean square error (RMSE) and goodness of fit (R^2) were calculated between the
161 model simulated values and original values. Internal validation was conducted on samples from odd years to evaluate the
162 fitting effect of the model, and cross validation was conducted on samples from even years to evaluate the simulation and
163 extrapolation effect of the model. The optimal phenology model for each species was selected based on the smallest RMSE
164 in cross validation and R^2 greater than 0.5 (0.3 for LCD) in both validations. If no model met these conditions, the species
165 was excluded when generating SP maps or GP maps.

166 For simulating SP maps, daily grid T data from ERA5-Land climate reanalysis were input into the optimal phenology
167 model and simulated pixel by pixel. This way, the phenology observations from individual sites were interpolated and
168 upscaled into a grid phenology map based on the phenology models (Chuine et al., 2000). However, as long as there was
169 grid T data, simulated species phenology could be obtained, even if there was no species distribution. Therefore, we named it
170 as species potential phenology map to avoid taking simulated values as true values in areas without species distribution.

171 **2.1.2 Species distribution maps**

172 In the second process, we simulated the species distribution maps using both species distribution models and county-
173 level species distribution data. Species distribution models were built for each species using Maximum Entropy Species
174 Distribution Modelling (Maxent; Phillips et al., 2006) version 3.4.4. Maxent estimates the range of a species by finding the
175 species distribution of maximum entropy (i.e., closest to the uniform), which is widely adopted in species distribution
176 modeling (Phillips et al., 2006). It expresses a probability distribution where each grid cell has a predicted probability of
177 presence for the species. To build the Maxent model, species location records from the GBIF database were used as
178 occurrence data input, and the 12 bioclimatic layers from BIOCLIM+ were used as the environmental data input. In the
179 model parameter settings, linear and quadratic feature types were used and 5-fold cross validation was used as the replicated
180 run type.

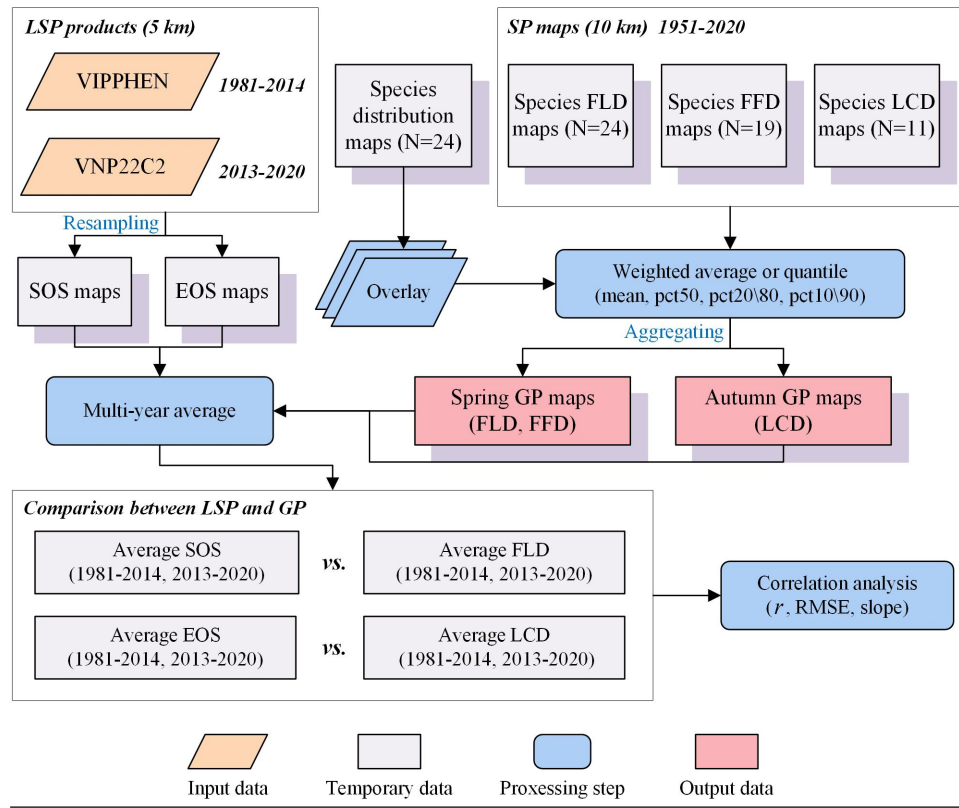
181 For model validation, the receiver operating characteristic (ROC) curve analysis method was used to test the accuracy
182 of the Maxent prediction model. The area under the ROC curve, known as the AUC value, is usually used as an indicator of
183 the prediction accuracy of the model (Fielding and Bell, 1997). The closer the AUC value is to 1.0, the more accurate the
184 prediction result of the model is. The average test AUC for different species was 0.845, with a standard deviation of 0.043
185 ([Table S2](#)).

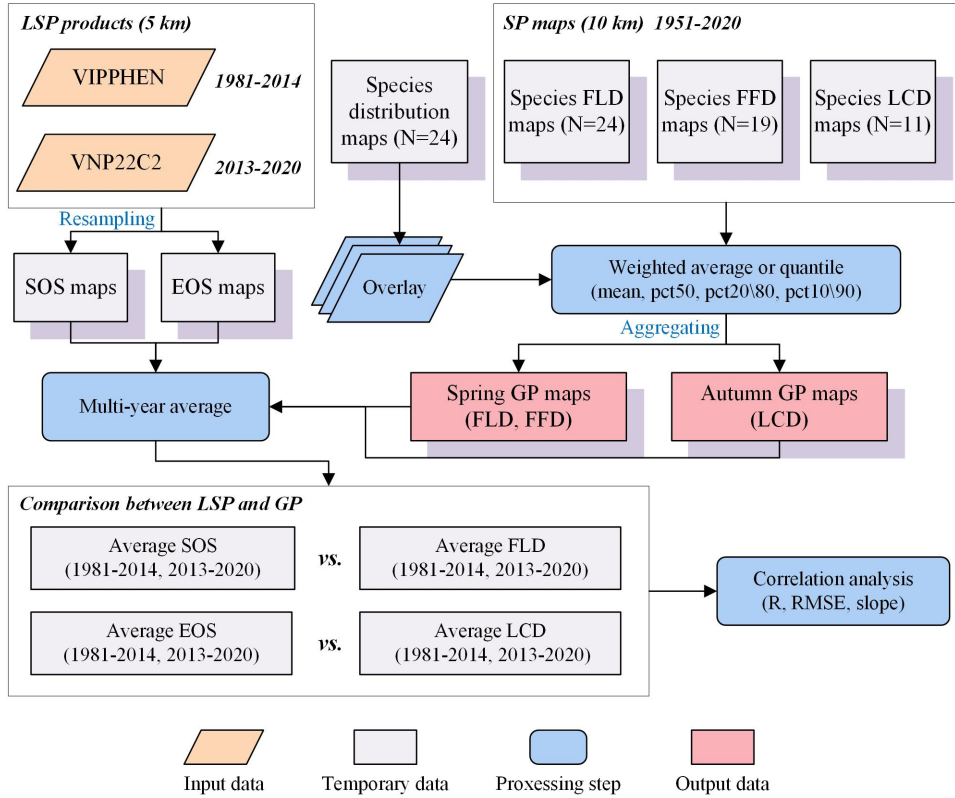
186 **2.3 Generating ground phenology maps using weighted average and weighted quantile methods**

187 We used four methods to aggregate from individual-level SP maps to landscape-level GP maps: (1) weighted average
188 (mean); (2) weighted median (pct50); (3) weighted 20th percentile (pct20) for spring phenology or weighted 80th percentile

189 (pct80) for autumn phenology; (4) weighted 10th percentile (pct10) for spring phenology or weighted 90th percentile (pct90)
190 for autumn phenology. Previous studies typically used species abundance as aggregation weights at the local scale, but it is
191 difficult to obtain such data at the regional scale. Therefore, we used species distribution probability instead of species
192 abundance as aggregation weight for each species. This assumption is based on a positive correlation between species
193 distribution and abundance (Brown, 1984), demonstrating that species tend to be most abundant at the center of their
194 geographic range (Sagarin and Gaines, 2002). The weight of each species was determined by the species distribution
195 probability, as it is assumed that the species abundance is positively related to the species distribution probability. The
196 aggregation methods of GP in this study (e.g., pct50, pct20\80 and pct10\90) are comparable and similar to the extraction
197 methods of LSP from remote sensing data (e.g., midpoint, dynamic threshold and maximum curvature). The workflow is
198 shown in Fig. 3.

199





201

202 **Figure 3:** The workflow of generating GP maps from SP maps, and comparing GP maps with two LSP products. The words
 203 in blue color represent the key processes of data generation.

204

205 For n species, the phenophases (Y) were first sorted from small to large. The SP of each species is y_i ($i = 1, 2, \dots, n$),
 206 and the distribution probability of each species is p_i ($i = 1, 2, \dots, n$). Then, the aggregated GP (Y_{mean} and Y_{pct} ($x\%$)) was
 207 calculated according to the following formulas:

$$208 \quad \omega_i = \frac{p_i}{\sum_{i=1}^n p_i} \quad (1)$$

$$209 \quad W_j = \sum_{i=1}^j \omega_i, j = 1, 2, \dots, n \quad (2)$$

$$210 \quad Y_{mean} = \sum_{i=1}^n \omega_i \times y_i \quad (3)$$

$$211 \quad Y_{pct} = \begin{cases} y_1, & \text{if } W_1 > x \\ (y_j - y_{j-1}) \times \frac{x - W_{j-1}}{\omega_j}, & \text{if } W_j > x, W_{j-1} < x \\ y_n, & \text{if } W_{n-1} < x \end{cases} \quad (4)$$

212 Where ω_i is the weight of each species, W_j is the cumulative weight from the first to the j species, $x\%$ is the percentile tag
213 which takes values from 10%, 20%, 50%, 80% and 90%. These formulas were used to calculate the aggregated GP maps by
214 combining the species phenology maps with the species distribution maps and weighting them by the species distribution
215 probability.

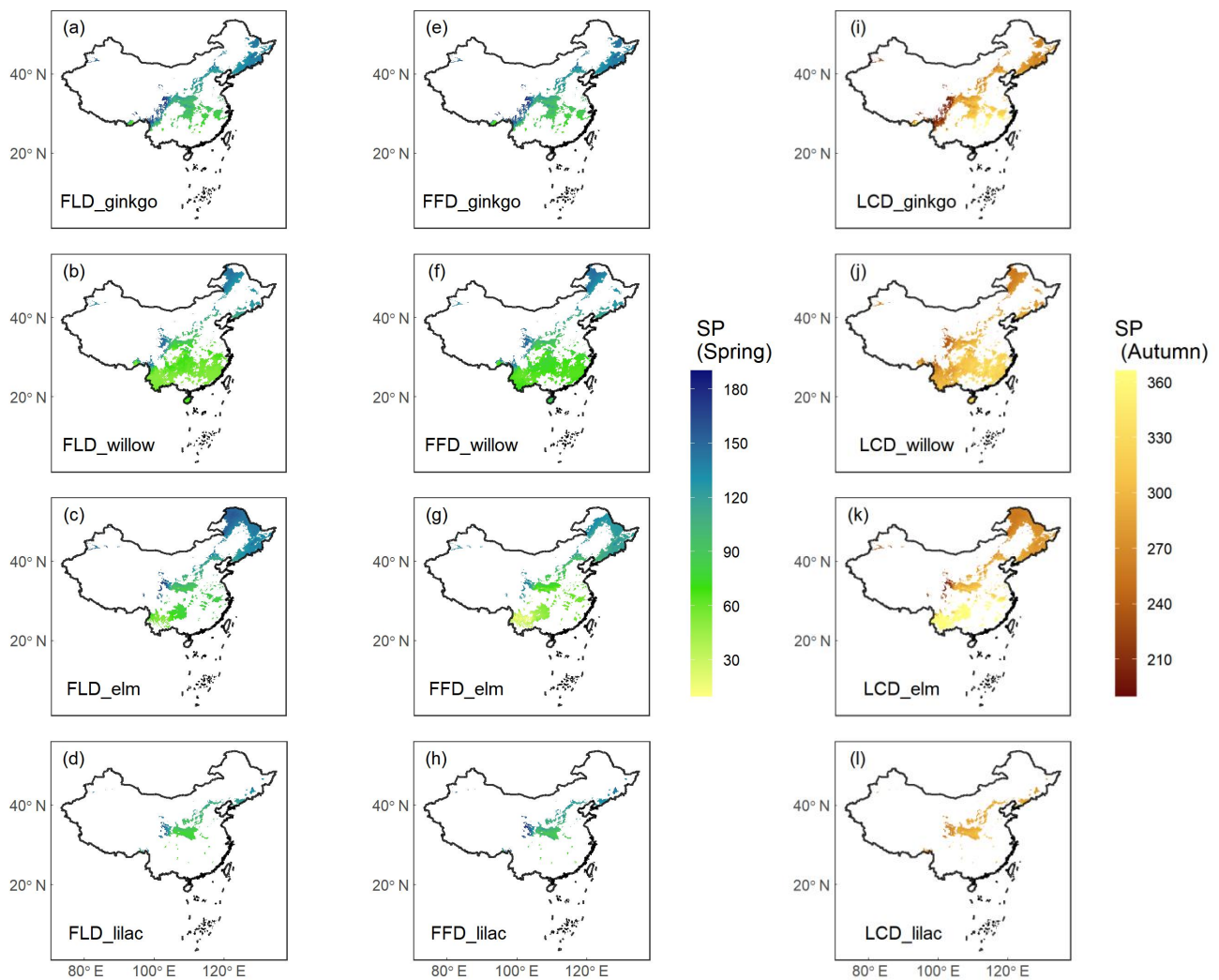
216 Finally, to assess data quality, the aggregated GP maps in this study were compared with two LSP products extracted
217 from remote sensing in previous studies ~~to assess data quality~~: (1) VIPPHEN_NDVI product (1981-2014), which used
218 midpoint method to extract the start of season (SOS) and the end of season (EOS) from the AVHRR data (Didan and
219 Barreto, 2016); (2) VNP22C2 product (2013-2020), which used maximum curvature method to extract SOS and EOS from
220 the MODIS data (Zhang et al., 2020b). Both LSP products were resampled from 5 km to 0.1° by the average method to
221 match the spatial resolution of GP maps. The LSP and GP maps were averaged in two segments (1981-2014 and 2013-
222 2020), and the correlation analysis was conducted between FLD and SOS in spring and between LCD and EOS in autumn.
223 Pearson correlation coefficient (R_r), RMSE, and linear regression slope were used to evaluate the consistency between GP
224 and LSP.

225 3 Results and discussion

226 The dataset includes two types of phenology maps over China: (1) Yearly SP maps generated by the model-based
227 upscaling method for 24 woody plants; (2) Yearly GP maps generated by four aggregation methods, along with the
228 corresponding quality assurance (QA) maps. The phenology maps provide spring FLD, FFD, and autumn LCD of woody
229 plants and forests over China from 1951 to 2020, with a spatial resolution of 0.1° and a temporal resolution of 1 day. Each
230 map is stored in a 16-bit signed integer file in GeoTIFF format, which contains a two-dimension raster (641 row \times 361
231 column). The unit of phenology data is the Julian Day of year (DOY), which represents the actual number of days from
232 January 1st to the date of phenology occurrence. The valid values range from DOY 1 to 366, and the null values equal to -1.

233 3.1 Simulation and validation of species phenology maps

234 The SP maps of FLD (24 species), FFD (19 species), and LCD (12 species) were simulated using the optimal
235 phenology models, and then masked by the species distribution maps. Here, we present the results of simulated SP maps of
236 four typical woody species (Fig. 4), including ginkgo (*Ginkgo biloba*), willow (*Salix babylonica*), elm (*Ulmus pumila*), and
237 lilac (*Syringa oblata*). These maps showed that the phenophases of different species have a consistent spatial pattern of
238 variation along latitude. Specifically, spring FLD and FFD of these species were significantly later with increasing latitude,
239 while autumn LCD was significantly earlier with increasing latitude. Despite similar spatial patterns, the phenophases of
240 different species show distinct temporal differences at the same latitude; for example, at lower latitudes, elm has
241 significantly earlier spring FFD and later autumn LCD than other species. Phenophases of some species were not simulated
242 because the R^2 of their optimal models was too small, e.g., $R^2 < 0.5$ for spring FFD, and $R^2 < 0.3$ for autumn LCD.



245 **Figure 4:** Species phenology (SP) maps of four typical woody species averaged from 1951 to 2020. Columns 1-2 show the
 246 spring phenophases (FLD and FFD), and Column 3 shows the autumn phenophase (LCD). Each row represents a species
 247 from ginkgo (*Ginkgo biloba*), willow (*Salix babylonica*), elm (*Ulmus pumila*), and lilac (*Syringa oblata*). The unit of
 248 **SPphenology data** is the Julian Day of year (DOY) from January 1st.

250 **Table 2:** The optimal phenology models and cross-validation results of 24 species. RMSE represents the root mean square
 251 error between the model simulated values and original values. R^2 represents goodness of fit of the optimal phenology model.

No.	Species	FLD	FFD	LCD
-----	---------	-----	-----	-----

		Optimal model	RMSE	R^2	Optimal model	RMSE	R^2	Optimal model	RMSE	R^2
1	<i>Ginkgo biloba</i>	TSC	7.30	0.669	TSC	7.53	0.553	DM	12.54	0.401
2	<i>Metasequoia glyptostroboides</i>	TSC	6.10	0.687	Unified	9.59	0.126	DM	9.99	0.295
3	<i>Magnolia denudata</i>	UniChill	6.47	0.781	TSC	7.33	0.576	DM	9.31	0.284
4	<i>Salix babylonica</i>	TSC	8.97	0.854	TSC	9.40	0.787	MR	18.23	0.380
5	<i>Populus × canadensis</i>	UniChill	5.94	0.808	UniChill	6.14	0.728	MR	9.45	0.139
6	<i>Robinia pseudoacacia</i>	TSC	5.47	0.863	TSC	6.18	0.785	DM	11.74	0.297
7	<i>Albizia julibrissin</i>	UniChill	7.48	0.500	Unified	8.23	0.376	MR	9.18	0.567
8	<i>Cercis chinensis</i>	TSC	7.90	0.723	UniChill	7.39	0.751	DM	9.09	0.175
9	<i>Prunus armeniaca</i>	TSC	6.05	0.865	UniChill	4.78	0.929	MR	14.52	0.191
10	<i>Ulmus pumila</i>	UniChill	5.09	0.901	UniChill	8.38	0.862	DM	11.16	0.654
11	<i>Morus alba</i>	TSC	6.70	0.905	UniChill	7.99	0.860	DM	9.04	0.175
12	<i>Broussonetia papyrifera</i>	UniChill	7.60	0.804	TSC	6.18	0.821	DM	9.97	0.615
13	<i>Quercus acutissima</i>	UniChill	6.73	0.931	UniChill	5.12	0.950	MR	14.35	0.765
14	<i>Pterocarya stenoptera</i>	UniChill	7.52	0.804	UniChill	7.89	0.710	MR	11.57	0.415
15	<i>Juglans regia</i>	TSC	6.04	0.739	UniChill	8.54	0.595	DM	8.41	0.141
16	<i>Betula platyphylla</i>	UniChill	3.80	0.915	UniChill	3.70	0.906	DM	8.27	0.655
17	<i>Acer pictum</i> subsp. <i>mono</i>	TSC	2.29	0.894	TSC	3.78	0.814	DM	4.71	0.670
18	<i>Ailanthus altissima</i>	UniChill	5.22	0.867	UniChill	8.34	0.664	DM	10.39	0.066
19	<i>Melia azedarach</i>	TSC	6.81	0.828	TSC	6.70	0.851	MR	10.19	0.135
20	<i>Firmiana simplex</i>	UniChill	6.02	0.694	Unified	8.10	0.314	DM	12.30	0.190
21	<i>Hibiscus syriacus</i>	TSC	9.66	0.666	Unified	13.38	0.331	DM	12.76	0.464
22	<i>Fraxinus chinensis</i>	TSC	6.25	0.852	Unified	12.35	0.319	MR	9.76	0.533
23	<i>Syringa oblata</i>	UniChill	7.01	0.864	UniChill	5.11	0.920	MR	12.36	0.475
24	<i>Paulownia fortunei</i>	UniChill	4.63	0.762	UniChill	7.02	0.693	MR	10.01	0.250

252

253

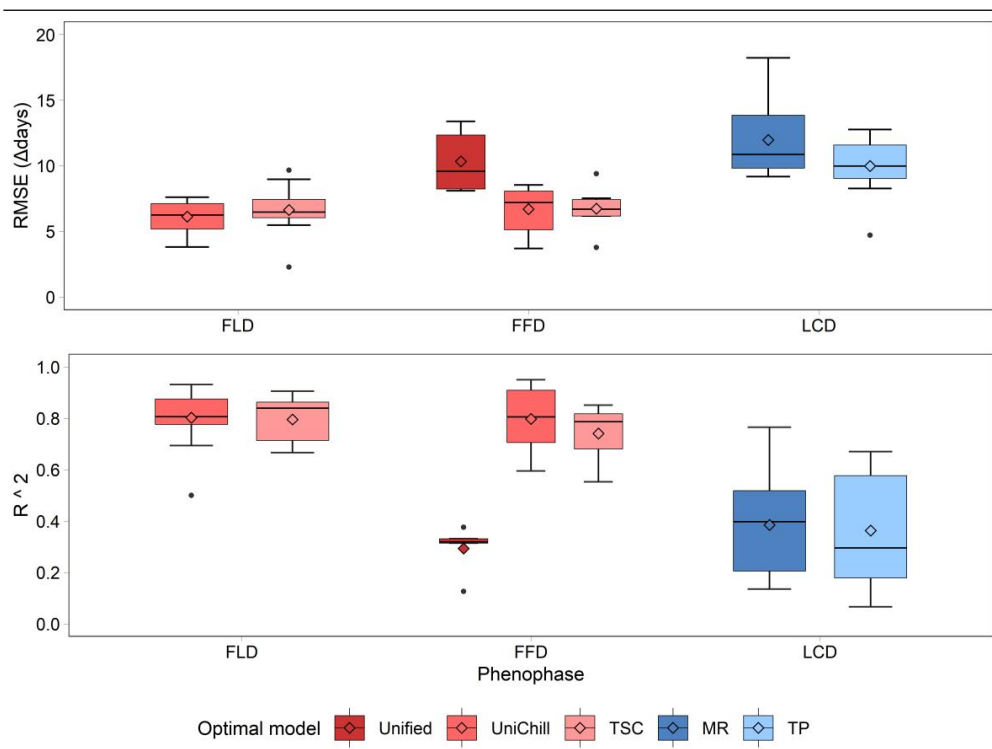
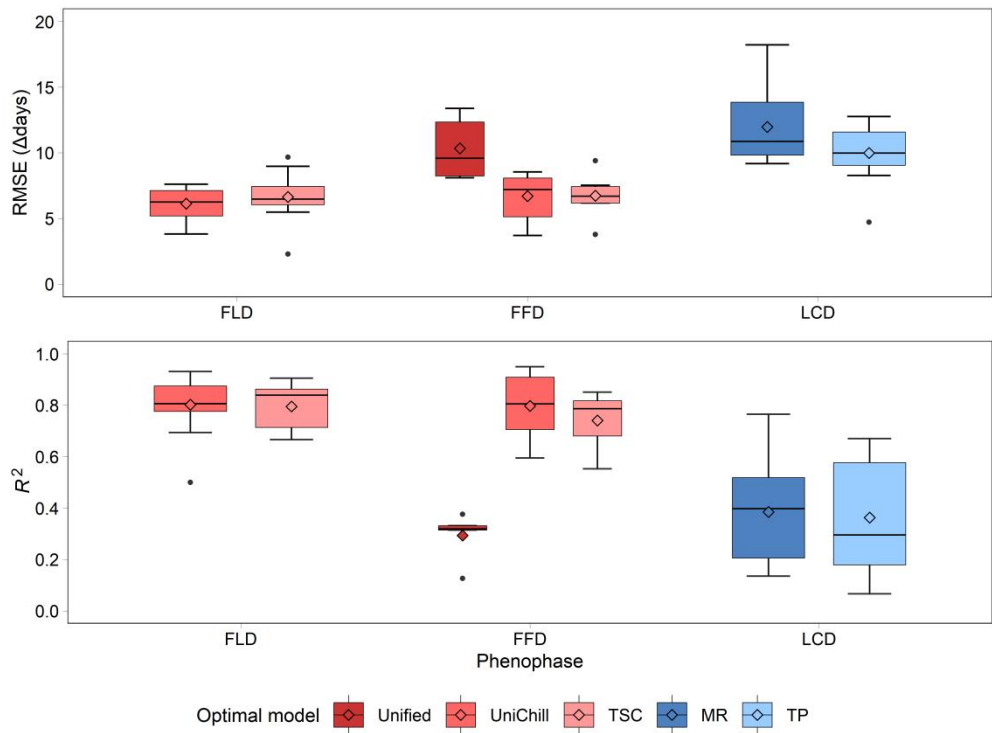
254

The simulation effects of species phenology maps were evaluated by cross-validation on the optimal phenology models

(Table 2). The results showed that the simulation effects of spring phenology were significantly better than that of autumn

255 phenology (Fig. 5). Specifically, the RMSE of the optimal model of FLD (6.38 days) and FFD (7.46 days) in spring were
256 significantly smaller than that of LCD (10.80 days) in autumn. And the R^2 of the optimal model of FLD (0.799) and FFD
257 (0.676) in spring were significantly greater than that of LCD (0.372) in autumn. However, there was no significant
258 difference between spring FLD and FFD simulation effects in spring. Among the optimal spring phenology models, the FFD
259 simulation effects of UniChill and TSC models were significantly better than Unified model. UniChill and TSC models, as
260 the optimal model, had significantly better FFD simulation effects than Unified models for the different phenology models in
261 spring. -But in autumn, the LCD simulations effects are similar for MR and TP models. MR and TP models had similar LCD-
262 simulation effects for the different phenology models in autumn.

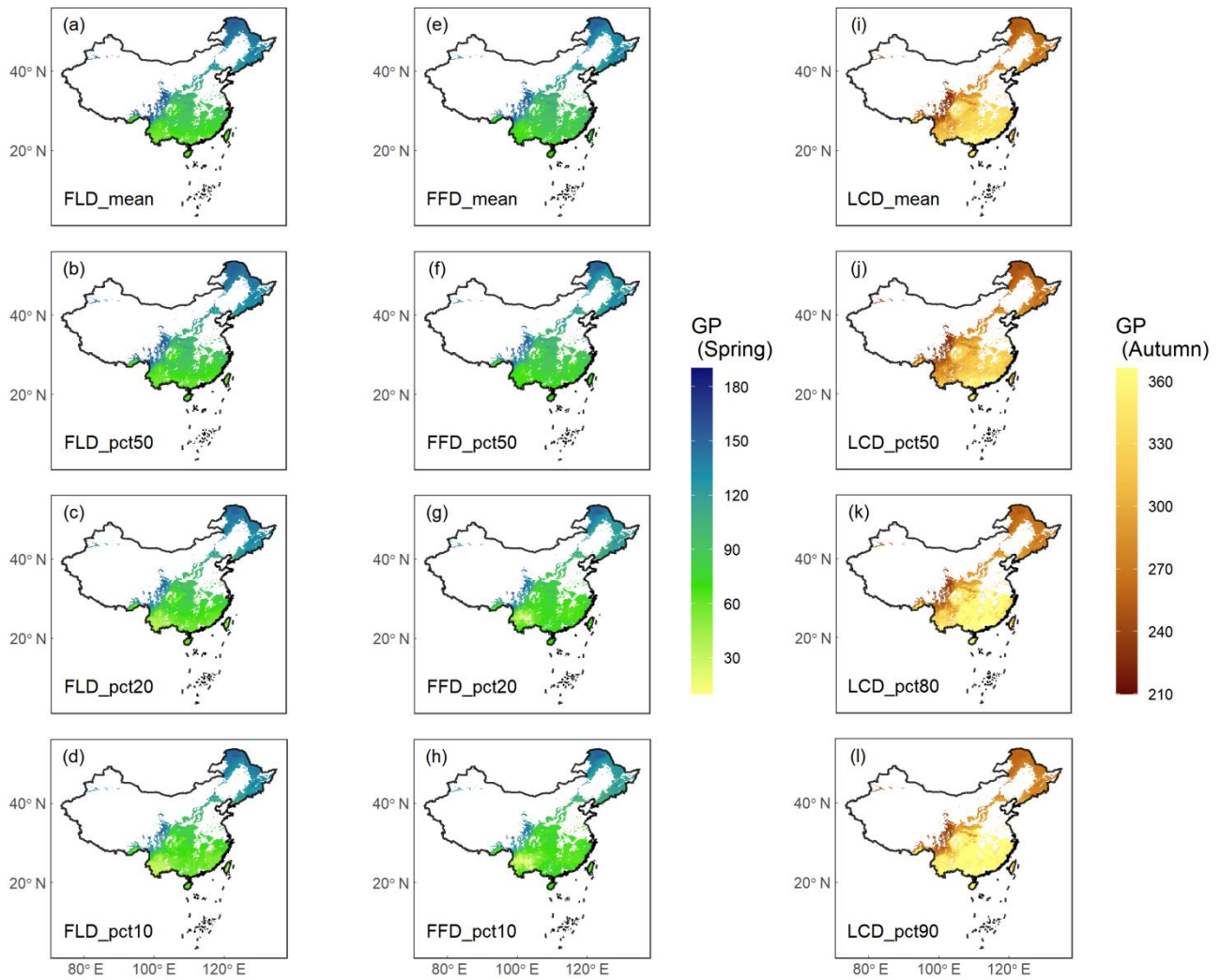
263



266 **Figure 5:** The RMSE (a) and R^2 (b) of cross-validation on the optimal phenology models for 24 woody species. Each model
267 is represented by a different color, with warm colors for three spring phenology models (Unified, UniChill, TSC), and cool
268 colors for two autumn phenology models (MR, TP). The model with the smallest RMSE was selected as the optimal model
269 for each species. The horizontal line represents the median value, the diamond mark represents the mean value, and the dot
270 mark represents the outlier in the boxplot.

271 **3.2 Aggregation of ground phenology maps**

272 The results of GP maps generated by four different aggregation methods (mean, pct50, pct20\80, pct10\90) showed
273 similar spatial patterns (Fig. 6), i.e., the consistent variation along latitude or altitude. With the increase of latitude or
274 altitude, the spring GP (FLD and FFD) became later, and the autumn GP (LCD) became earlier. For different aggregation
275 methods, the GP maps aggregated from the mean and pct50 methods were highly consistent, with R_r being 0.992; while the
276 GP maps aggregated from the pct20\80 and pct10\90 methods were slightly different from the former two, with R_r being
277 0.968 and 0.949, and showed larger spatial variation than the former two. The high consistency between the mean and pct50
278 maps indicated that both the weighted mean method and weighted quantile method were robust for the aggregation of GP.
279



280

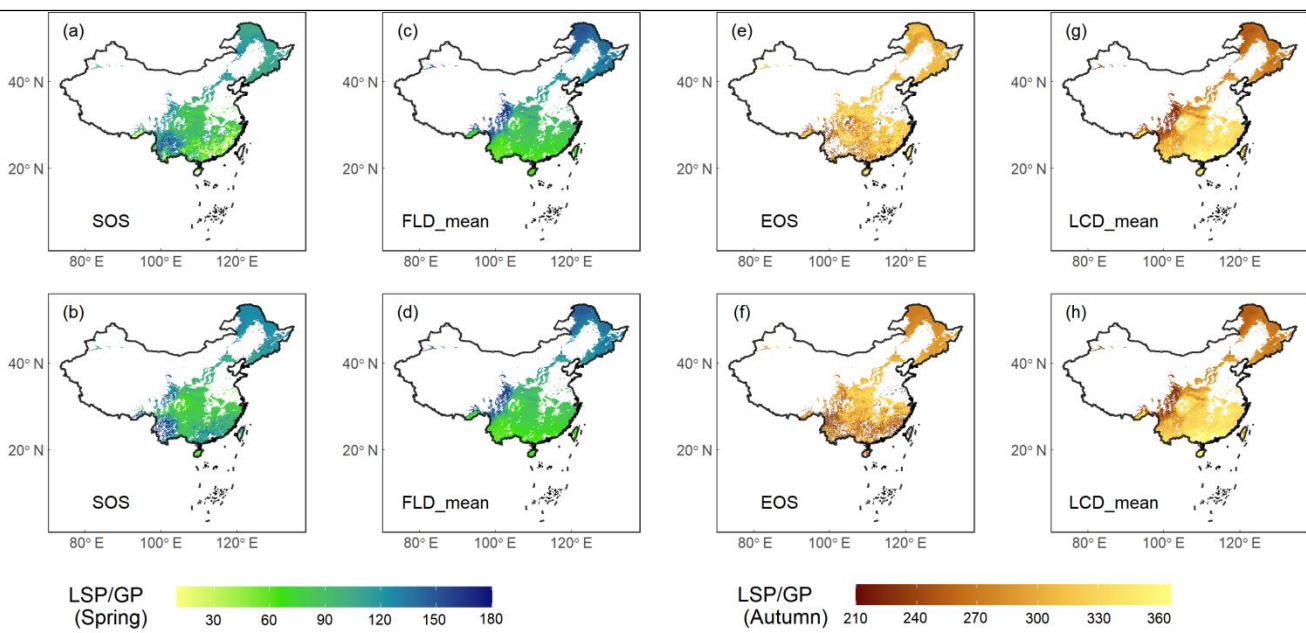
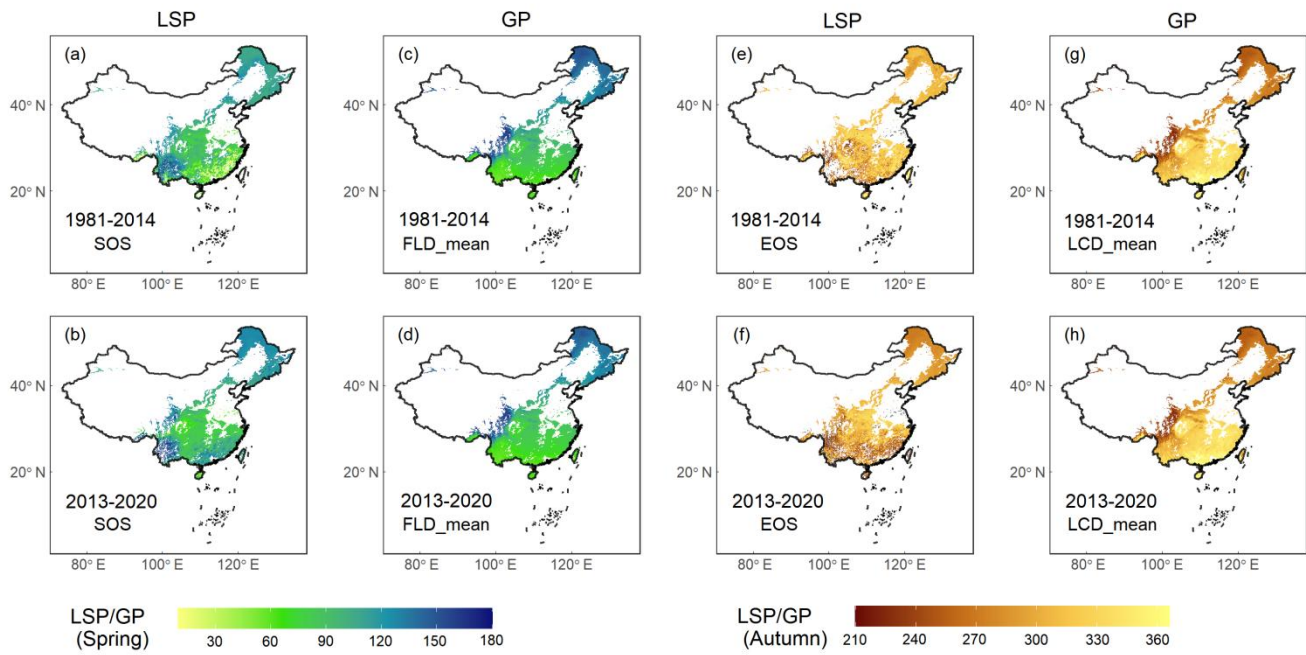
281 **Figure 6:** Ground phenology (GP) maps of four aggregation methods averaged from 1951 to 2020. Columns 1-2 show the
 282 spring phenophases (FLD and FFD), and Column 3 shows the autumn phenophase (LCD). Each row represents an
 283 aggregation method from weighted average (mean), weighted median (pct50), weighted 20% or 80% percentile (pct20\80),
 284 and weighted 10% or 90% percentile (pct10\90). The unit of GP is the Julian Day of year (DOY) from January 1st.
 285

286 We also provided two QA maps to evaluate the reliability of the aggregation results of GP maps (Fig. S1). The first is
 287 the total distribution probability of all species, and the second is the total number of species with distribution probabilities
 288 greater than 0.1. In the QA maps, higher values mean larger total number or probability of species for the aggregation,
 289 indicating that GP maps have higher reliability in these areas. The regions with the most reliable GP aggregation results were
 290 distributed around 30° N in China. The total number of species is about 15 for FLD and FFD, and is about 6 for LCD in

291 these regions. It should be noted that in the QA map, in areas where the total number of species is less than 5 or the total
292 probability of species is less than 1, the aggregation results of GP may not be reliable.

293 **3.3 Data quality and usability**

294 GP and LSP were compared between FLD and SOS in spring and between LCD and EOS in autumn during two
295 segments (1981-2014 and 2013-2020). The results showed that GP and two LSP products had similar spatial patterns in
296 central and northern China but relatively different patterns in southern China (Fig. 7), particularly for LCD and EOS in
297 autumn (Fig. 7e-h). This is likely due to the prevalence of deciduous forests-(~~DF~~) in central and northern China (Fig. 1). In
298 contrast, evergreen-~~forests (EF)~~ and mixed forests-(~~MF~~) are found in southern China. GP in this study was generated by
299 aggregating the ~~SPphenology~~ of 24 deciduous woody plants, which made up a large proportion of ~~DF~~ deciduous forests but
300 a small proportion of evergreen or mixed forests~~EF or MF~~. Additionally, LSP extracted from remote sensing data tends to
301 have a larger error in evergreen and mixed forests~~EF and MF~~ due to the lack of obvious seasonal change and frequent cloud
302 cover in these regions (Liu et al., 2016b). As a result, the consistency between GP and LSP was relatively poor in evergreen
303 or mixed forests~~EF and MF areas~~ (Fig. S2), with the maximum *R_r* being 0.44 in spring and 0.54 in autumn, and the
304 minimum RMSE being 28.5 days in spring and 38.5 days in autumn (Table S2). In contrast, the consistency between GP and
305 LSP was much better in ~~DF~~ deciduous forests~~area~~, with the maximum *R_r* being 0.95 in spring and 0.88 in autumn, and the
306 minimum RMSE being 8.8 days in spring and 15.1 days in autumn, respectively.



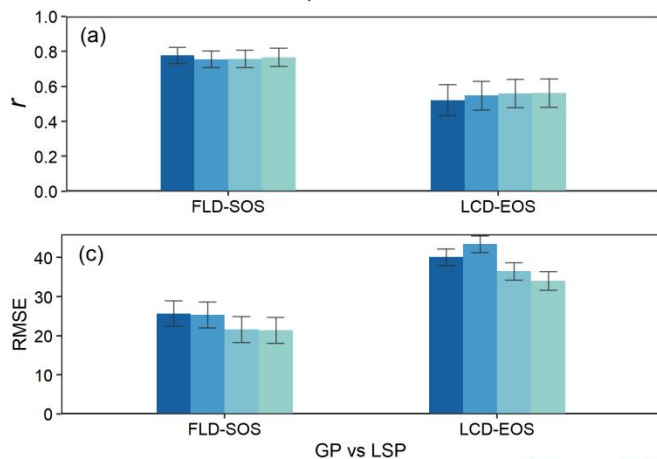
309 **Figure 7:** Comparison of GP maps in this study and two LSP products (VIPPHEN and VNP22C2) extracted from remote
 310 sensing in previous studies, which was made between FLD and SOS in spring and LCD and EOS in autumn. Row 1 shows
 311 the comparison between VIPPHEN product and GP map averaged in 1981-2014, and Row 2 shows the comparison between
 312 VNP22C2 product and GP map averaged in 2013-2020. (a-b) SOS from two LSP products; (c-d) FLD aggregated by mean

313 method; (e-f) EOS from two LSP products; (g-h) LCD aggregated by mean method. The unit of GP or LSP is the Julian Day
314 of year (DOY) from January 1st.

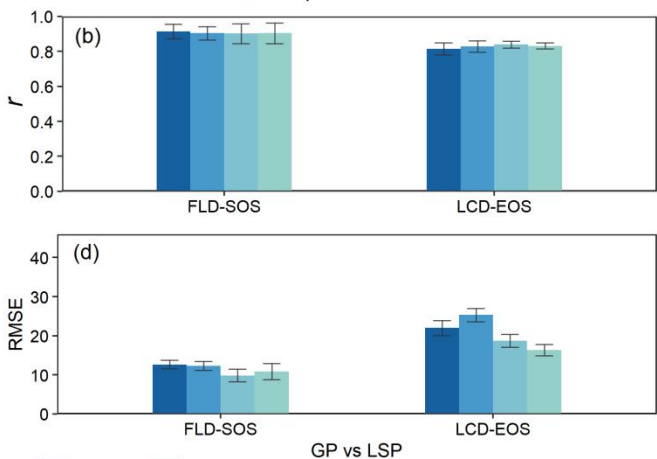
315

316 To further assess the quality of the data, we examined the consistency between GP and LSP specifically in ~~DF areas~~
317 deciduous forests. The results showed that GP and LSP had good consistency ~~in DF areas~~ for both VIPPHEN and VNP22C2
318 products, i.e., high correlation (R), small difference ($RMSE$), and good linear relationship (Fig. 8). Compared with the LSP
319 of VIPPHEN product, the LSP of VNP22C2 product has better consistency with the GP of this study. In addition, for both
320 products, the consistency between GP and LSP in spring (Fig. 8e, g) was significantly better than that in autumn (Fig. 8f, h).
321 When comparing different aggregation methods (mean, pct50, pct20/80, pct10/90), there was no significant difference in Rr
322 between GP and LSP (Fig. 8a, b). All methods produced similar Rr values, ranging from 0.76-0.78 in spring and 0.49-0.53 in
323 autumn for the VIPPHEN product, and from 0.90-0.91 in spring and 0.79-0.84 in autumn for the VNP22C2 product.
324 However, different methods produced significantly different RMSE values between GP and LSP (Fig. 8c, d), largely due to
325 the differences in the average values of GP under different methods. The best aggregation methods, with the minimum
326 RMSE, were pct10 (20.8 days) in spring and pct90 (32.9 days) in autumn for the VIPPHEN product, and pct20 (8.8 days) in
327 spring and pct90 (15.1 days) in autumn for the VNP22C2 product.

VIPPHEN product (1981-2014)

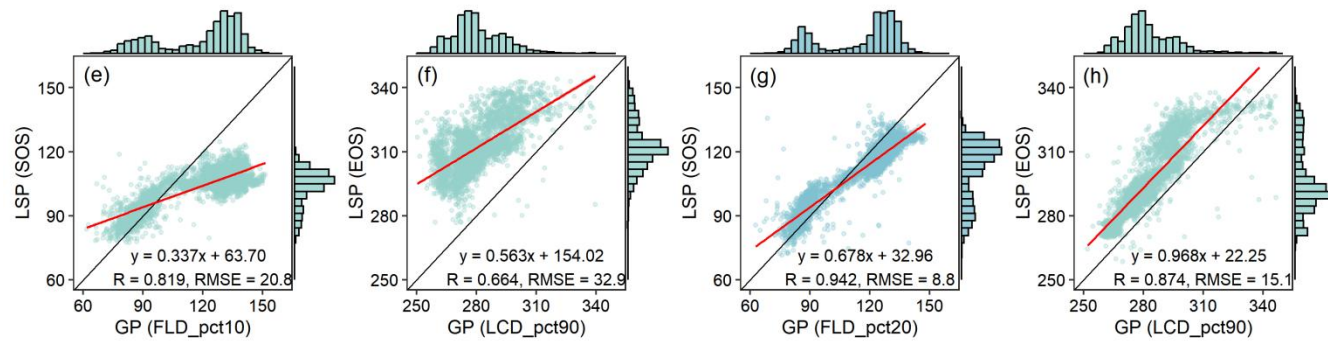


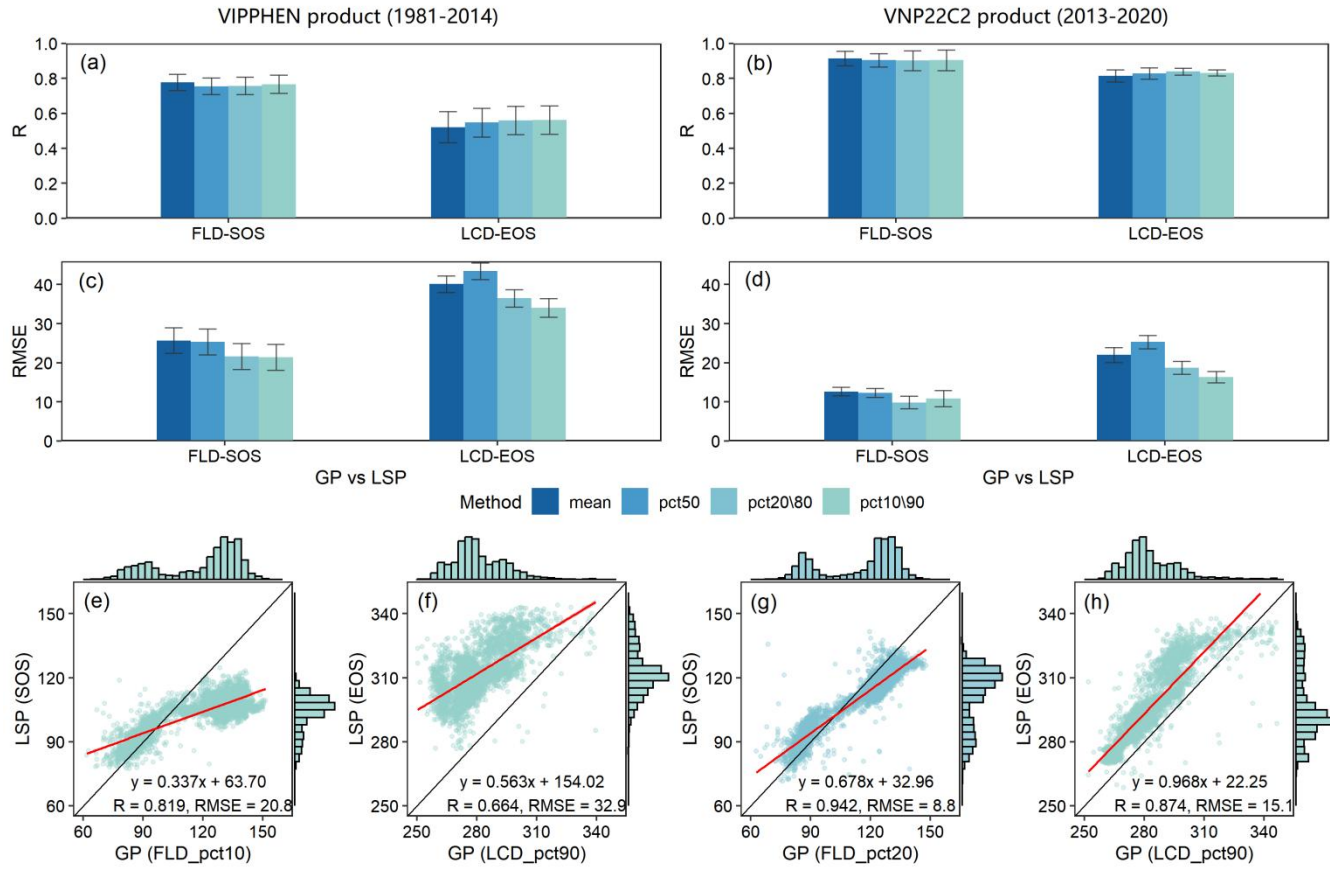
VNP22C2 product (2013-2020)



GP vs LSP

Method mean pct50 pct20|80 pct10|90





329
330 **Figure 8:** Comparison results of GP maps and two LSP products (VIPPHEN and VNP22C2) in ~~DF areas~~ **deciduous forests**,
331 which was made between FLD and SOS in spring and LCD and EOS in autumn within the time range 1981-2014 and 2013-
332 2020. (a-b) R_r between LSP and GP under four aggregating methods; (c-d) RMSE between LSP and GP under four
333 aggregating methods; (e-h) Linear relationship between between LSP and GP under the best aggregating method. Each
334 aggregating method is represented by a different color. The best aggregating method was determined by minimizing the
335 RMSE between GP and LSP ~~in DF areas~~. The error bar in the bar plot represents the multi-year standard deviation. The red
336 line in the scatter plot represents the linear regression line between GP and LSP, and all regression results were extremely
337 significant ($p < 0.001$).

338
339 It is worth noting that the aggregation method with the smallest difference between GP and LSP in this study was the
340 10th or 20th percentile in spring and the 90th percentile in autumn. It means that the spring green-up event detected by
341 remote sensing is more consistent with the FLD of earlier-developing plant species (the first 10%-20%) on the ground, while
342 the autumn dormancy event from remote sensing is more consistent with the LCD of later-senescing plant species (the last

343 10%) on the ground. These results reveal a potential connection between GPs and LSPs despite their different physical
344 implications in diagnosing phenology.

345 In general, this dataset provides high reliability ~~SP and GP~~species and ground phenology simulations of forests over
346 China for the past 70 years. It is an independent phenology data source generated by the modeling and aggregation based on
347 ground observations. There are several considerations in data application:

348 (1) For SP maps, the accuracy of data was determined by RMSE and R^2 of cross-validation on the optimal phenology
349 model for each species (Table 2). Additionally, the reliability of ~~SP~~phenology data in space was affected by the number of
350 sites available for modeling on each species (Table 1). For instance, the accuracy of *Betula platyphylla*'s FLD was very high
351 overall (RMSE = 3.80 and R^2 = 0.915), but the local accuracy might be relatively poor in areas with sparse sites due to very
352 few sites of *Betula platyphylla* in space ($n = 13$). In this study, the SP maps of 24 species in China were found to be largely
353 consistent with the in-situ observations, with an average error of 6.4, 7.5 and 10.8 days for FLD, FFD and LCD,
354 respectively. These errors were the same or smaller than those of phenology modelling in previous studies. For example, the
355 simulation error of spring FLD and FFD was 7-9 days in central Europe (Basler, 2016) and was 12.3-12.7 days in the United
356 States (Izquierdo-Verdiguier et al., 2018), while the simulation error of autumn LCD was 10.3-13.0 days in France
357 (Delpierre et al., 2009) and 5.9-22.8 days in the United States (Jeong and Medvigy, 2014). Therefore, compared with other
358 studies on the regional scale, the SP maps of China in this study were found to have relatively high accuracy.

359 (2) For GP maps, the reliability of data can be determined by QA maps which provide the total number or probability of
360 species. Additionally, the reliability can also be evaluated by comparing GP data with other LSP products, with high
361 consistency indicating good reliability. Since GP data actually provide phenology estimates of the ~~deciduous~~DF components
362 in the forests, it has better reliability in the ~~DF areas~~deciduous forests but less reliability in ~~evergreen or mixed forests~~EF or
363 ~~MF areas~~. In this study, GP maps of forests in China were found have good consistency with the existing LSP products,
364 particularly in ~~DF area~~deciduous forestss, where the correlation coefficients of FLD and LCD were 0.91 and 0.84,
365 respectively. The differences between GP and LSP in FLD and LCD were also found to be relatively small in ~~DF area~~
366 deciduous forests, being 8.8 days and 15.1 days, respectively. Previous studies have shown poor consistency between single
367 species and LSP, with correlation coefficients ranging from 0.50 to 0.51 in the United States (Peng et al., 2017) and
368 Germany (Kowalski et al., 2020), and differences ranging from 12 to 14.5 days in the United States (Peng et al., 2017) and
369 Canada (Delbart et al., 2015). In contrast, research comparing average or quantile values of multiple species has shown
370 better results similar to this study. For example, the correlation coefficients between the average (or weighted average) GP
371 and LSP were found to be 0.61 to 0.71 in Europe (Rodriguez-Galiano et al., 2015; Tian et al., 2021). The correlation
372 coefficients between the 30th percentile GP and LSP were found to be 0.54 to 0.57 in China (Wu et al., 2016). The
373 differences between the GP and LSP in previous studies were 10.3-12.4 days in China (Wu et al., 2016), 13.9 days in
374 Europe, and 12.3 days in the United States (Ye et al., 2022), which was larger than the results of FLD but smaller than that
375 of LCD in this study. Although the landscape-level GP data aggregated from species-level ~~SP~~phenology data in this study

376 showed good reliability, limitations in available species and different aggregation methods suggest that future comparisons
377 between GP and LSP in other regions still need to be improved.

378 (3) For phenology maps in different seasons, the reliability of phenology data in spring was found to be significantly
379 higher than that in autumn. The underlying reason is that the mechanism of autumn phenology is more complex compared to
380 that of spring phenology (Menzel, 2002). Moreover, the driving mechanisms for influencing factors of the autumn phenology
381 are complex not yet fully understood, which poses an additional challenge (Gill et al., 2015; Wu et al., 2018). For example,
382 temperature has large effects on the autumn phenology than the spring phenology (Fu et al., 2018). In addition to
383 temperature, other environmental factors such as precipitation (An et al., 2020), photoperiod (Lang et al., 2019), solar
384 radiation (Wu et al., 2021b), spring phenology (Liu et al., 2016a), and growing-season productivity (Zani et al., 2020) may
385 also drive autumn phenology. Thus, modeling autumn phenology is more challenging compared to spring phenology
386 (Melaas et al., 2016), resulting in poorer model performance and inferior data quality of SP or GP maps in autumn.

387 4 Data availability

388 The annual SP and GP maps over China can be accessed at <https://doi.org/10.57760/sciencedb.07995> (Zhu et al., 2023).
389 This dataset is licensed under a CC-BY 4.0 license. The spatial reference system of the dataset is EPSG:4326(WGS84).

390 5 Conclusions

391 In this study, mainly based on CPON historical phenology observations, we developed a new long-term gridded
392 phenology dataset: SP maps of 24 woody plants and GP maps of forests over China from 1951–2020, with a spatial
393 resolution of 0.1° and a temporal resolution of 1 day. For the generation of SP maps, we adopted a model-based upscaling
394 method to realize the scale expansion of SPphenology date from in-situ to regional scales in China. For the generation of GP
395 maps, we adopted weighted average and weighted quantile methods to realize the aggregation from species to community or
396 landscape levels in China. Dataset quality assessment shows that the average error of SP maps is 6.9 days in spring and 10.8
397 days in autumn, and the minimum difference between GP maps and existing LSP products is 8.8 days in spring and 15.1
398 days in autumn. Compared to the previous studies (Basler, 2016; Delpierre et al., 2009; Izquierdo-Verdiguier et al., 2018;
399 Jeong and Medvigy, 2014; Tian et al., 2021; Wu et al., 2016; Ye et al., 2022), the SP maps in this study have the same or
400 smaller simulation error, and the GP maps in this study have good agreement with other LSP products, so the data has high
401 accuracy and reliability. This dataset is the first phenology map of China. It can be used to investigate the spatial pattern of
402 plant phenology more clearly along the geographic gradient (e.g., longitude, latitude, and altitude), and to reveal the
403 temporal trends (e.g., interannual, decadal, and secular) of plant phenology across China. The dataset can also provide
404 important data support for global change impact assessment, terrestrial ecosystem simulation, and natural resource
405 management.

406 **Author contribution**

407 QG and JD designed the study and planned the modeling. HW developed the model code. WL and YH performed the
408 simulations. MZ processed the modeling data, performed the computations and drafted the manuscript. JD and JA critically
409 revised the manuscript. All authors discussed and contributed to the modeling and manuscript.

410 **Competing interests**

411 The authors declare that they have no conflict of interest.

412 **Acknowledgements**

413 This study was jointly supported by National Key Research and Development Program of China (2018YFA0606102),
414 National Natural Science Foundation of China (42271062), and Strategic Priority Research Program (A) of Chinese
415 Academy of Sciences (XDA19020303; XDA26010202). Phenology data was provided by CPON. Temperature data was
416 provided by Copernicus Climate Change Service (C3S).

417 **References**

418 An, S., Chen, X., Zhang, X., Lang, W., Ren, S., and Xu, L.: Precipitation and minimum temperature are primary climatic
419 controls of alpine grassland autumn phenology on the Qinghai-Tibet Plateau, *Remote Sens.*, 12, 431,
420 <https://doi.org/10.3390/rs12030431>, 2020.

421 Aono, Y. and Kazui, K.: Phenological data series of cherry tree flowering in Kyoto, Japan, and its application to
422 reconstruction of springtime temperatures since the 9th century, *Int. J. Climatol.*, 28, 905–914,
423 <https://doi.org/10.1002/joc.1594>, 2008.

424 Ault, T. R., Schwartz, M. D., Zurita-Milla, R., Weltzin, J. F., and Betancourt, J. L.: Trends and natural variability of spring
425 onset in the coterminous United States as evaluated by a new gridded dataset of spring indices, *J. Clim.*, 28, 8363–8378,
426 <https://doi.org/10.1175/jcli-d-14-00736.1>, 2015.

427 Basler, D.: Evaluating phenological models for the prediction of leaf-out dates in six temperate tree species across central
428 Europe, *Agric. For. Meteorol.*, 217, 10–21, <https://doi.org/10.1016/j.agrformet.2015.11.007>, 2016.

429 Bolton, D. K., Gray, J. M., Melaas, E. K., Moon, M., Eklundh, L., and Friedl, M. A.: Continental-scale land surface
430 phenology from harmonized Landsat 8 and Sentinel-2 imagery, *Remote Sens. Environ.*, 240, 111685,
431 <https://doi.org/10.1016/j.rse.2020.111685>, 2020.

432 Brown, J. H.: On the Relationship between Abundance and Distribution of Species, *Am. Nat.*, 124, 255–279,
433 <https://doi.org/10.1086/284267>, 1984.

434 Brun, P., Zimmermann, N., Hari, C., Pellissier, L., and Karger, D.: CHELSA-BIOCLIM+ A novel set of global climate-
435 related predictors at kilometre-resolution, EnviDat [data set], 10, 2022a.

436 Brun, P., Zimmermann, N. E., Hari, C., Pellissier, L., and Karger, D. N.: Global climate-related predictors at kilometer
437 resolution for the past and future, *Earth Syst. Sci. Data*, 14, 5573–5603, <https://doi.org/10.5194/essd-14-5573-2022>,
438 2022b.

439 Cai, H., Lyu, L., Shrestha, N., Tang, Z., Su, X., Xu, X., Dimitrov, D., and Wang, Z.: Geographical patterns in phylogenetic
440 diversity of Chinese woody plants and its application for conservation planning, *Divers. Distrib.*, 27, 179–194,
441 <https://doi.org/10.1111/ddi.13180>, 2021.

442 Chuine, I.: A unified model for budburst of trees, *J. Theor. Biol.*, 207, 337–347, <https://doi.org/10.1006/jtbi.2000.2178>,
443 2000.

444 Chuine, I., Cour, P., and Rousseau, D.: Fitting models predicting dates of flowering of temperate-zone trees using simulated
445 annealing, *Plant Cell Environ.*, 21, 455–466, <https://doi.org/10.1046/j.1365-3040.1998.00299.x>, 1998.

446 Chuine, I., Cambon, G., and Comtois, P.: Scaling phenology from the local to the regional level: advances from species-
447 specific phenological models, *Global Change Biol.*, 6, 943–952, <https://doi.org/10.1046/j.1365-2486.2000.00368.x>,
448 2000.

449 Cleland, E. E., Chuine, I., Menzel, A., Mooney, H. A., and Schwartz, M. D.: Shifting plant phenology in response to global
450 change, *Trends Ecol. Evol.*, 22, 357–365, <https://doi.org/10.1016/j.tree.2007.04.003>, 2007.

451 Dai, J., Wang, H., and Ge, Q.: Multiple phenological responses to climate change among 42 plant species in Xi'an, China,
452 *Int. J. Biometeorol.*, 57, 749–758, <https://doi.org/10.1007/s00484-012-0602-2>, 2013.

453 Dai, J., Wang, H., and Ge, Q.: Characteristics of spring phenological changes in China over the past 50 years, *Adv.
454 Meteorol.*, 2014, 1–8, <https://doi.org/10.1155/2014/843568>, 2014.

455 Delbart, N., Beaubien, E., Kergoat, L., and Le Toan, T.: Comparing land surface phenology with leafing and flowering
456 observations from the PlantWatch citizen network, *Remote Sens. Environ.*, 160, 273–280,
457 <https://doi.org/10.1016/j.rse.2015.01.012>, 2015.

458 Delpierre, N., Dufrêne, E., Soudani, K., Ulrich, E., Cecchini, S., Boé, J., and François, C.: Modelling interannual and spatial
459 variability of leaf senescence for three deciduous tree species in France, *Agric. For. Meteorol.*, 149, 938–948,
460 <https://doi.org/10.1016/j.agrformet.2008.11.014>, 2009.

461 Didan, K. and Barreto, A.: NASA MEaSUREs Vegetation Index and Phenology (VIP) Phenology NDVI Yearly Global
462 0.05Deg CMG, NASA EOSDIS Land Processes DAAC, accessed on 2022-08-11,
463 https://doi.org/10.5067/MEaSUREs/VIP/VIPPHEN_NDVI.004, 2016.

464 Dixon, D. J., Callow, J. N., Duncan, J. M., Setterfield, S. A., and Pauli, N.: Satellite prediction of forest flowering
465 phenology, *Remote Sens. Environ.*, 255, 112197, <https://doi.org/10.1016/j.rse.2020.112197>, 2021.

466 Donnelly, A., Yu, R., Jones, K., Belitz, M., Li, B., Duffy, K., Zhang, X., Wang, J., Seyednasrollah, B., Gerst, K. L., and
467 others: Exploring discrepancies between in situ phenology and remotely derived phenometrics at NEON sites,
468 *Ecosphere*, 13, e3912, <https://doi.org/10.1002/ecs2.3912>, 2022.

469 Dronova, I. and Taddeo, S.: Remote sensing of phenology: Towards the comprehensive indicators of plant community
470 dynamics from species to regional scales, *J. Ecol.*, 110, 1460–1484, <https://doi.org/10.1111/1365-2745.13897>, 2022.

471 Estrella, N. and Menzel, A.: Responses of leaf colouring in four deciduous tree species to climate and weather in Germany,
472 *Clim. Res.*, 32, 253–267, <https://doi.org/10.3354/cr032253>, 2006.

473 Fang, J., Wang, Z., and Tang, Z.: *Atlas of woody plants in China: distribution and climate*, Springer Science & Business
474 Media, 2011.

475 Fielding, A. H. and Bell, J. F.: A review of methods for the assessment of prediction errors in conservation presence/absence
476 models, *Environ. Conserv.*, 24, 38–49, <https://doi.org/10.1017/s0376892997000088>, 1997.

477 Fisher, J. I., Mustard, J. F., and Vadeboncoeur, M. A.: Green leaf phenology at Landsat resolution: Scaling from the field to
478 the satellite, *Remote Sens. Environ.*, 100, 265–279, <https://doi.org/10.1016/j.rse.2005.10.022>, 2006.

479 Fitchett, J. M., Grab, S. W., and Thompson, D. I.: Plant phenology and climate change: Progress in methodological
480 approaches and application, *Prog. Phys. Geogr.*, 39, 460–482, <https://doi.org/10.1177/0309133315578940>, 2015.

481 Friedl, M. and Sulla-Menashe, D.: MODIS/Terra+Aqua Land Cover Type Yearly L3 Global 500m SIN Grid V061, NASA
482 EOSDIS Land Processes DAAC, <https://doi.org/10.5067/MODIS/MCD12Q1.061>, 2022.

483 Fu, Y., Li, X., Zhou, X., Geng, X., Guo, Y., and Zhang, Y.: Progress in plant phenology modeling under global climate
484 change, *Sci. China Earth Sci.*, 63, 1237–1247, <https://doi.org/10.1007/s11430-019-9622-2>, 2020.

485 Fu, Y. H., Zhao, H., Piao, S., Peaucelle, M., Peng, S., Zhou, G., Ciais, P., Huang, M., Menzel, A., Peñuelas, J., and others:
486 Declining global warming effects on the phenology of spring leaf unfolding, *Nature*, 526, 104–107,
487 <https://doi.org/10.1038/nature15402>, 2015.

488 Fu, Y. H., Piao, S., Delpierre, N., Hao, F., Hänninen, H., Liu, Y., Sun, W., Janssens, I. A., and Campioli, M.: Larger
489 temperature response of autumn leaf senescence than spring leaf-out phenology, *Global Change Biol.*, 24, 2159–2168,
490 <https://doi.org/10.1111/gcb.14021>, 2018.

491 Ganguly, S., Friedl, M. A., Tan, B., Zhang, X., and Verma, M.: Land surface phenology from MODIS: Characterization of
492 the Collection 5 global land cover dynamics product, *Remote Sens. Environ.*, 114, 1805–1816,
493 <https://doi.org/10.1016/j.rse.2010.04.005>, 2010.

494 GBIF: GBIF Occurrence Download, accessed on 2022-08-12, <https://doi.org/10.15468/dl.7dwjev>, 2022.

495 Ge, Q., Wang, H., and Dai, J.: Simulating changes in the leaf unfolding time of 20 plant species in China over the twenty-
496 first century, *Int. J. Biometeorol.*, 58, 473–484, <https://doi.org/10.1007/s00484-013-0671-x>, 2014.

497 Ge, Q., Wang, H., Rutishauser, T., and Dai, J.: Phenological response to climate change in China: a meta-analysis, *Global
498 Change Biol.*, 21, 265–274, <https://doi.org/10.1111/gcb.12648>, 2015.

499 Gill, A. L., Gallinat, A. S., Sanders-DeMott, R., Rigden, A. J., Short Gianotti, D. J., Mantooth, J. A., and Templer, P. H.:
500 Changes in autumn senescence in northern hemisphere deciduous trees: a meta-analysis of autumn phenology studies,
501 *Ann Bot*, 116, 875–888, <https://doi.org/10.1093/aob/mcv055>, 2015.

502 Hufkens, K., Basler, D., Milliman, T., Melaas, E. K., and Richardson, A. D.: An integrated phenology modelling framework
503 in R, *Methods Ecol. Evol.*, 9, 1276–1285, <https://doi.org/10.1111/2041-210x.12970>, 2018.

504 ~~Inouye, D. W.: Climate change and phenology, Wiley Interdiscip. Rev. Clim. Change, 13, e764,~~
505 <https://doi.org/10.1002/wee.764>, 2022.

506 Izquierdo-Verdiguier, E., Zurita-Milla, R., Ault, T. R., and Schwartz, M. D.: Development and analysis of spring plant
507 phenology products: 36 years of 1-km grids over the conterminous US, *Agric. For. Meteorol.*, 262, 34–41,
508 <https://doi.org/10.1016/j.agrformet.2018.06.028>, 2018.

509 Jeong, S.-J. and Medvigy, D.: Macroscale prediction of autumn leaf coloration throughout the continental United States,
510 *Global Ecol. Biogeogr.*, 23, 1245–1254, <https://doi.org/10.1111/geb.12206>, 2014.

511 Keenan, T. F., Gray, J., Friedl, M. A., Toomey, M., Bohrer, G., Hollinger, D. Y., Munger, J. W., O’Keefe, J., Schmid, H. P.,
512 Wing, I. S., and others: Net carbon uptake has increased through warming-induced changes in temperate forest
513 phenology, *Nat. Clim. Change*, 4, 598–604, <https://doi.org/10.1038/nclimate2253>, 2014.

514 Kowalski, K., Senf, C., Hostert, P., and Pflugmacher, D.: Characterizing spring phenology of temperate broadleaf forests
515 using Landsat and Sentinel-2 time series, *Int. J. Appl. Earth Obs. Geoinf.*, 92, 102172,
516 <https://doi.org/10.1016/j.jag.2020.102172>, 2020.

517 Lang, W., Chen, X., Qian, S., Liu, G., and Piao, S.: A new process-based model for predicting autumn phenology: how is
518 leaf senescence controlled by photoperiod and temperature coupling?, *Agric. For. Meteorol.*, 268, 124–135,
519 <https://doi.org/10.1016/j.agrformet.2019.01.006>, 2019.

520 Li, X., Zhou, Y., Meng, L., Asrar, G. R., Lu, C., and Wu, Q.: A dataset of 30 m annual vegetation phenology indicators
521 (1985–2015) in urban areas of the conterminous United States, *Earth Syst. Sci. Data*, 11, 881–894,
522 <https://doi.org/10.5194/essd-11-881-2019>, 2019.

523 Liang, L., Schwartz, M. D., and Fei, S.: Validating satellite phenology through intensive ground observation and landscape
524 scaling in a mixed seasonal forest, *Remote Sens. Environ.*, 115, 143–157, <https://doi.org/10.1016/j.rse.2010.08.013>,
525 2011.

526 ~~Lieth, H.: Purposes of a phenology book, in: Phenology and Seasonality Modeling, edited by: Lieth, H., Springer, Berlin,~~
527 ~~Heidelberg, 3–19, https://doi.org/10.1007/978-3-642-51863-8_1, 1974.~~

528 ~~Lieth, H.: Purposes of a phenology book, in: Phenology and Seasonality Modeling, Springer-Verlag, New York, 3–19, 1974.~~

529 Liu, H., Gong, P., Wang, J., Clinton, N., Bai, Y., and Liang, S.: Annual dynamics of global land cover and its long-term
530 changes from 1982 to 2015, *Earth Syst. Sci. Data*, 12, 1217–1243, <https://doi.org/10.5194/essd-12-1217-2020>, 2020.

531 Liu, Q., Fu, Y. H., Zhu, Z., Liu, Y., Liu, Z., Huang, M., Janssens, I. A., and Piao, S.: Delayed autumn phenology in the
532 Northern Hemisphere is related to change in both climate and spring phenology, *Global Change Biol.*, 22, 3702–3711,
533 <https://doi.org/10.1111/gcb.13311>, 2016a.

534 Liu, Y., Wu, C., Peng, D., Xu, S., Gonsamo, A., Jassal, R. S., Arain, M. A., Lu, L., Fang, B., and Chen, J. M.: Improved
535 modeling of land surface phenology using MODIS land surface reflectance and temperature at evergreen needleleaf
536 forests of central North America, *Remote Sens. Environ.*, 176, 152–162, <https://doi.org/10.1016/j.rse.2016.01.021>,
537 2016b.

538 Melaas, E. K., Sulla-Menashe, D., Gray, J. M., Black, T. A., Morin, T. H., Richardson, A. D., and Friedl, M. A.: Multisite
539 analysis of land surface phenology in North American temperate and boreal deciduous forests from Landsat, *Remote*
540 *Sens. Environ.*, 186, 452–464, <https://doi.org/10.1016/j.rse.2016.09.014>, 2016.

541 Menzel, A.: Phenology: its importance to the global change community, *Clim. Change*, 54, 379,
542 <https://doi.org/10.1023/A:1016125215496>, 2002.

543 Menzel, A., Yuan, Y., Matiu, M., Sparks, T., Scheifinger, H., Gehrig, R., and Estrella, N.: Climate change fingerprints in
544 recent European plant phenology, *Global Change Biol.*, 26, 2599–2612, <https://doi.org/10.1111/gcb.15000>, 2020.

545 Misra, G., Cawkwell, F., and Wingler, A.: Status of phenological research using Sentinel-2 data: A review, *Remote Sens.*,
546 12, 2760, <https://doi.org/10.3390/rs12172760>, 2020.

547 Muñoz Sabater, J.: ERA5-Land hourly data from 1981 to present, Copernicus Climate Change Service (C3S) Climate Data
548 Store (CDS), 2019.

549 Muñoz Sabater, J.: ERA5-Land hourly data from 1950 to 1980, Copernicus Climate Change Service (C3S) Climate Data
550 Store (CDS), 2021.

551 Muñoz-Sabater, J., Dutra, E., Agustí-Panareda, A., Albergel, C., Arduini, G., Balsamo, G., Boussetta, S., Choulga, M.,
552 Harrigan, S., Hersbach, H., and others: ERA5-Land: A state-of-the-art global reanalysis dataset for land applications,
553 *Earth Syst. Sci. Data*, 13, 4349–4383, <https://doi.org/10.5194/essd-13-4349-2021>, 2021.

554 Nasahara, K. N. and Nagai, S.: [Development of an in-situ observation network for terrestrial ecological remote sensing: the Phenological Eyes Network \(PEN\)](https://doi.org/10.1007/s11284-014-1239-x), *Ecol. Res.*, 30, 211–223, <https://doi.org/10.1007/s11284-014-1239-x>, 2015.

556 Park, D. S., Newman, E. A., and Breckheimer, I. K.: Scale gaps in landscape phenology: challenges and opportunities,
557 *Trends Ecol. Evol.*, 36, 709–721, <https://doi.org/10.1016/j.tree.2021.04.008>, 2021.

558 Peng, D., Wu, C., Li, C., Zhang, X., Liu, Z., Ye, H., Luo, S., Liu, X., Hu, Y., and Fang, B.: Spring green-up phenology
559 products derived from MODIS NDVI and EVI: Intercomparison, interpretation and validation using National Phenology
560 Network and AmeriFlux observations, *Ecol. Indic.*, 77, 323–336, <https://doi.org/10.1016/j.ecolind.2017.02.024>, 2017.

561 Phillips, S. J., Anderson, R. P., and Schapire, R. E.: Maximum entropy modeling of species geographic distributions, *Ecol.*
562 *Modell.*, 190, 231–259, <https://doi.org/10.1016/j.ecolmodel.2005.03.026>, 2006.

563 Piao, S., Liu, Q., Chen, A., Janssens, I. A., Fu, Y., Dai, J., Liu, L., Lian, X., Shen, M., and Zhu, X.: Plant phenology and
564 global climate change: Current progresses and challenges, *Glob Chang Biol*, 25, 1922–1940,
565 <https://doi.org/10.1111/gcb.14619>, 2019.

566 Polgar, C. A. and Primack, R. B.: Leaf-out phenology of temperate woody plants: from trees to ecosystems, *New Phytol.*,
567 191, 926–941, <https://doi.org/10.1111/j.1469-8137.2011.03803.x>, 2011.

568 **Pukelsheim, F.: The three sigma rule, *Am. Stat.*, 48, 88–91, <https://doi.org/10.2307/2684253>, 1994.**

569 Richardson, A. D., Keenan, T. F., Migliavacca, M., Ryu, Y., Sonnentag, O., and Toomey, M.: Climate change, phenology,
570 and phenological control of vegetation feedbacks to the climate system, *Agric. For. Meteorol.*, 169, 156–173,
571 <https://doi.org/10.1016/j.agrformet.2012.09.012>, 2013.

572 Richardson, A. D., Hufkens, K., Milliman, T., Aubrecht, D. M., Chen, M., Gray, J. M., Johnston, M. R., Keenan, T. F.,
573 Klosterman, S. T., Kosmala, M., and others: Tracking vegetation phenology across diverse North American biomes
574 using PhenoCam imagery, *Sci. Data*, 5, 1–24, <https://doi.org/10.1038/sdata.2018.28>, 2018.

575 Rodriguez-Galiano, V., Dash, J., and Atkinson, P. M.: Intercomparison of satellite sensor land surface phenology and ground
576 phenology in Europe, *Geophys. Res. Lett.*, 42, 2253–2260, <https://doi.org/10.1002/2015gl063586>, 2015.

577 **Sagarin, R. D. and Gaines, S. D.: The ‘abundant centre’ distribution: to what extent is it a biogeographical rule?, *Ecol. Lett.*,**
578 **5, 137–147, <https://doi.org/10.1046/j.1461-0248.2002.00297.x>, 2002.**

579 Schwartz, M. D.: Phenology: an integrative environmental science, Springer, 2003.

580 **Schwartz, M. D., Betancourt, J. L., and Weltzin, J. F.: From Caprio’s lilaes to the USA national phenology network, *Front.*
581 *Ecol. Environ.*, 10, 324–327, <https://doi.org/10.1890/110281>, 2012.**

582 **Schwartz, M. D., Ault, T. R., and Betancourt, J. L.: Spring onset variations and trends in the continental United States: past
583 and regional assessment using temperature-based indices, *Int. J. Climatol.*, 33, 2917–2922,
584 <https://doi.org/10.1002/joc.3625>, 2013.**

585 Studer, S., Stöckli, R., Appenzeller, C., and Vidale, P. L.: A comparative study of satellite and ground-based phenology, *Int.*
586 *J. Biometeorol.*, 51, 405–414, <https://doi.org/10.1007/s00484-006-0080-5>, 2007.

587 Tang, J., Körner, C., Muraoka, H., Piao, S., Shen, M., Thackeray, S. J., and Yang, X.: Emerging opportunities and
588 challenges in phenology: a review, *Ecosphere*, 7, e01436, <https://doi.org/10.1002/ecs2.1436>, 2016.

589 Tao, Z., Wang, H., Dai, J., Alatalo, J., and Ge, Q.: Modeling spatiotemporal variations in leaf coloring date of three tree
590 species across China, *Agric. For. Meteorol.*, 249, 310–318, <https://doi.org/10.1016/j.agrformet.2017.10.034>, 2018.

591 Templ, B., Koch, E., Bolmgren, K., Ungersböck, M., Paul, A., Scheifinger, H., Rutishauser, T., Busto, M., Chmielewski, F.-
592 M., Hájková, L., and others: Pan European Phenological database (PEP725): a single point of access for European data,
593 *Int. J. Biometeorol.*, 62, 1109–1113, <https://doi.org/10.1007/s00484-018-1512-8>, 2018.

594 Tian, F., Cai, Z., Jin, H., Hufkens, K., Scheifinger, H., Tagesson, T., Smets, B., Van Hoolst, R., Bonte, K., Ivits, E., and
595 others: Calibrating vegetation phenology from Sentinel-2 using eddy covariance, PhenoCam, and PEP725 networks
596 across Europe, *Remote Sens. Environ.*, 260, 112456, <https://doi.org/10.1016/j.rse.2021.112456>, 2021.

597 Wang, H., Dai, J., and Ge, Q.: The spatiotemporal characteristics of spring phenophase changes of *Fraxinus chinensis* in
598 China from 1952 to 2007, *Sci. China Earth Sci.*, 55, 991–1000, <https://doi.org/10.1007/s11430-011-4349-0>, 2012.

599 ~~Wang, H., Ge, Q., Rutishauser, T., Dai, Y., and Dai, J.: Parameterization of temperature sensitivity of spring phenology and~~
600 ~~its application in explaining diverse phenological responses to temperature change, *Sci. Rep.*, 5, 8833,~~
601 ~~<https://doi.org/10.1038/srep08833>, 2015.~~

602 Wang, H., Wu, C., Ciais, P., Peñuelas, J., Dai, J., Fu, Y., and Ge, Q.: Overestimation of the effect of climatic warming on
603 spring phenology due to misrepresentation of chilling, *Nat. Commun.*, 11, 4945, [https://doi.org/10.1038/s41467-020-18743-8](https://doi.org/10.1038/s41467-020-
604 18743-8), 2020a.

605 ~~Wang, L., Tian, F., Huang, K., Wang, Y., Wu, Z., and Fensholt, R.: Asymmetric patterns and temporal changes in~~
606 ~~phenology-based seasonal gross carbon uptake of global terrestrial ecosystems, *Global Ecol. Biogeogr.*, 29, 1020–1033,~~
607 ~~<https://doi.org/10.1111/geb.13084>, 2020b.~~

608 Wu, C., Hou, X., Peng, D., Gonsamo, A., and Xu, S.: Land surface phenology of China's temperate ecosystems over 1999–
609 2013: Spatial–temporal patterns, interaction effects, covariation with climate and implications for productivity,
610 *Agricultural and Forest Meteorology*, 216, 177–187, <https://doi.org/10.1016/j.agrformet.2015.10.015>, 2016.

611 Wu, C., Wang, X., Wang, H., Ciais, P., Peñuelas, J., Myneni, R. B., Desai, A. R., Gough, C. M., Gonsamo, A., Black, A. T.,
612 and others: Contrasting responses of autumn-leaf senescence to daytime and night-time warming, *Nat. Clim. Change*, 8,
613 1092–1096, <https://doi.org/10.1038/s41558-018-0346-z>, 2018.

614 Wu, W., Sun, Y., Xiao, K., and Xin, Q.: Development of a global annual land surface phenology dataset for 1982–2018 from
615 the AVHRR data by implementing multiple phenology retrieving methods, *Int. J. Appl. Earth Obs. Geoinf.*, 103,
616 102487, <https://doi.org/10.1016/j.jag.2021.102487>, 2021a.

617 Wu, Z., Chen, S., De Boeck, H. J., Stenseth, N. C., Tang, J., Vittasse, Y., Wang, S., Zohner, C., and Fu, Y. H.: Atmospheric
618 brightening counteracts warming-induced delays in autumn phenology of temperate trees in Europe, *Global Ecol.*
619 *Biogeogr.*, 30, 2477–2487, <https://doi.org/10.1111/geb.13404>, 2021b.

620 Ye, Y., Zhang, X., Shen, Y., Wang, J., Crimmins, T., and Scheifinger, H.: An optimal method for validating satellite-derived
621 land surface phenology using in-situ observations from national phenology networks, *ISPRS J. Photogramm. Remote*
622 *Sens.*, 194, 74–90, <https://doi.org/10.1016/j.isprsjprs.2022.09.018>, 2022.

623 Zani, D., Crowther, T. W., Mo, L., Renner, S. S., and Zohner, C. M.: Increased growing-season productivity drives earlier
624 autumn leaf senescence in temperate trees, *Science*, 370, 1066–1071, <https://doi.org/10.1126/science.abd8911>, 2020.

625 Zhang, X., Wang, J., Gao, F., Liu, Y., Schaaf, C., Friedl, M., Yu, Y., Jayavelu, S., Gray, J., Liu, L., and others: Exploration
626 of scaling effects on coarse resolution land surface phenology, *Remote Sens. Environ.*, 190, 318–330,
627 <https://doi.org/10.1016/j.rse.2017.01.001>, 2017.

628 ~~Zhang, X., Wang, J., Henebry, G. M., and Gao, F.: Development and evaluation of a new algorithm for detecting 30-m land-~~
629 ~~surface phenology from VIIRS and HLS time series, *ISPRS J. Photogramm. Remote Sens.*, 161, 37–51,~~
630 ~~<https://doi.org/10.1016/j.isprsjprs.2020.01.012>, 2020a.~~

631 Zhang, X., Friedl, M., and Henebry, G.: VIIRS/NPP Land Cover Dynamics Yearly L3 Global 0.05 Deg CMG V001, NASA
632 EOSDIS Land Processes DAAC, accessed on 2022-08-11, <https://doi.org/10.5067/VIIRS/VNP22C2.001>, 2020^b. |

633 Zhu, M., Dai J.: Species phenology and ground phenology maps over China from 1951-2020, Science Data Bank [data set],
634 <https://doi.org/10.57760/sciencedb.07995>. DOI:10.57760/sciencedb.07995, 2023.